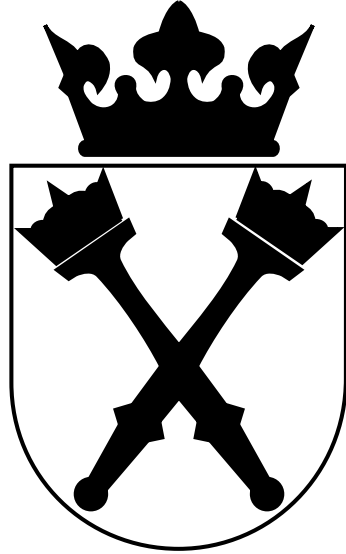


Jagiellonian University

MARIAN SMOLUCHOWSKI INSTITUTE OF PHYSICS



Assembly and measurements
of the Electromagnetic Calorimeter components
for “WASA at COSY” setup

Benedykt Jany

Master Thesis prepared at the Nuclear Physics Department
Supervisor: Dr. hab. Zbigniew Rudy

Cracow 2006

“QUOD SCIMUS, GUTTA EST, IGNORAMUS MARE.”

Abstract

This work describes the tests of the scintillator electromagnetic calorimeter of the WASA detector setup after transferring it from the CELSIUS storage ring at The Svedberg Laboratory(Uppsala, Sweden) to the Cooler Synchrotron COSY at the Institut für Kernphysik (IKP) of Forschungszentrum Jülich, Germany. The tests were performed using gammas of 4.4MeV energy from an AmBe source. The status of the CsI(Na) crystals was determined and the indication of gain factor for the energy calibration was extracted.

Streszczenie

Ta praca magisterska opisuje testy kalorymetru elektromagnetycznego detektora WASA po jego transferze z akceleratora CELSIUS The Svedberg Laboratory (Uppsala, Szwecja) do Forschungszentrum Jülich Institut für Kernphysik (IKP) Niemcy (akcelerator COSY). Testy zostały przeprowadzone przy użyciu źródła Amerykowo-Berylowego emitującego promienie gamma o energii 4.4 MeV. Kryształy CsI(Na) zostały sprawdzone oraz stałe kalibracyjne zostały wyliczone.

Contents

1	Introduction	5
2	The WASA at COSY Project	7
2.1	Cooler Synchrotron COSY	7
2.2	The WASA detector	10
2.2.1	The Pellet Target	11
2.2.2	The Forward Detector	13
2.2.3	The Central Detector	14
2.3	Physics at WASA	19
3	Physics of Calorimetry	23
3.1	Some definitions	23
3.2	The electromagnetic calorimeter itself	28
4	Measurements of the WASA calorimeter	33
4.1	Electronics setup	33
4.2	General Analysis	36
4.3	Source measurements	38
4.4	Cosmics measurements	44
5	Summary and conclusions	51
	References	56
	Appendix A	59

1 Introduction

This work was performed during my stay from November 2005 to April 2006 in the Institut für Kernphysik (IKP) of Forschungszentrum Jülich, Germany as a diploma student of the Jagiellonian University Cracow. It was motivated by the transfer of the WASA[6] detector setup from the CELSIUS storage ring at TSL(Uppsala, Sweden) to the Cooler Synchrotron COSY at IKP [1]. This latter results in an unique scientific opportunities for hadron physics with hadronic probes: COSY with its phase-space cooled proton and deuteron beams covering an energy region up to the ϕ -meson sector is combined with WASA, a close to 4π detector for photons and charged particles. After the transfer to Jülich and prior to installation in the COSY ring - which is scheduled for summer 2006 - all detectors needed to be tested and to be tuned. This thesis deals with the electromagnetic calorimeter of WASA, probably the most important and most crucial part of the whole setup.

The thesis is divided into three main parts. Section 2 describes the advantages of the transfer WASA to Jülich[2], and gives an overview over the WASA detector including the pellet target system. Special attention was put to the central part and particularly to the electromagnetic calorimeter.

Section 3 reveals the physics of electromagnetic interactions of photons and electrons with matter. Basic issues of calorimeter physics are given.

Section 4 describes the performed measurements on the calorimeter. Section 4.1 shows how the data were taken and a description of electronics is presented. The general analysis of the data is introduced in section 4.2. Finally section 4.3 is dealing with the main goal of this thesis, the test of the CsI(Na) calorimeter crystals with 4.4MeV gamma source. Section 4.4 provides a comparison with energy deposits by cosmic muons in the calorimeter medium, using a Monte-Carlo simulation of the full WASA setup.

A Summary with conclusions are given in section 5 – future implications for the WASA calorimeter are considered.



2 The WASA at COSY Project

The WASA detector setup had been operated since 1998. It has been built with the focus on studying the decays of η -mesons in nuclear reactions. However, in 2003 it has been decided to shut down the CELSIUS ring thus, to stop the operation of WASA at CELSIUS. Shortly after that announcement the idea came up to continue the operation of WASA at COSY. The reasons are obvious: The combination of WASA and COSY would be of advantages for both communities. COSY offers a higher energy than CELSIUS, allowing the extension of the studies into the η' sector. The WASA detector had an electromagnetic calorimeter as a central component and, thus, the ability to detect neutral decay modes involving photons – such a device is missing at COSY. The proposal [2] for moving WASA to COSY was accepted by the COSY PAC in 2004. The WASA detector was dismantled during summer 2005 and shipped to Jülich. The final installation is scheduled for summer 2006.

2.1 Cooler Synchrotron COSY



Figure 1: View at the Cooler Synchrotron COSY.

The Cooler Synchrotron COSY Fig. 1 is located in the IKP of the Forschungszentrum Jülich Germany. It delivers phase-space cooled polarized or unpolarized protons (deuterons) of momentum from $p = 300$ MeV/c up to $p = 3700$ MeV/c. The ring has a circumference of 184m and can be filled with up to 10^{11} particles. When using the internal cluster target the luminosity of value $10^{31}\text{cm}^{-2}\text{s}^{-1}$ can be reached. Two cooling methods are applied during accumulation of the beam to reduce the phase-space volume, electron cooling at injection energies and stochastic cooling. In the electron cooling method an electron beam, moving with the same average velocity as proton beam, absorbs the kinetic energy of protons, whereas stochastic cooling is the process in which the deviations of nominal energy or position of particles in a beam are measured and corrected. The electron cooling system in COSY is applied at injection momentum $p = 300$ MeV/c and reaches up to $p = 600$ MeV/c, and the stochastic cooling from $p = 1500$ MeV/c to 3700 MeV/c. Both, proton and deuteron beams, can be provided unpolarized as well as polarized. At COSY internal and external target positions are in operation Fig. 2. For further details see [8].

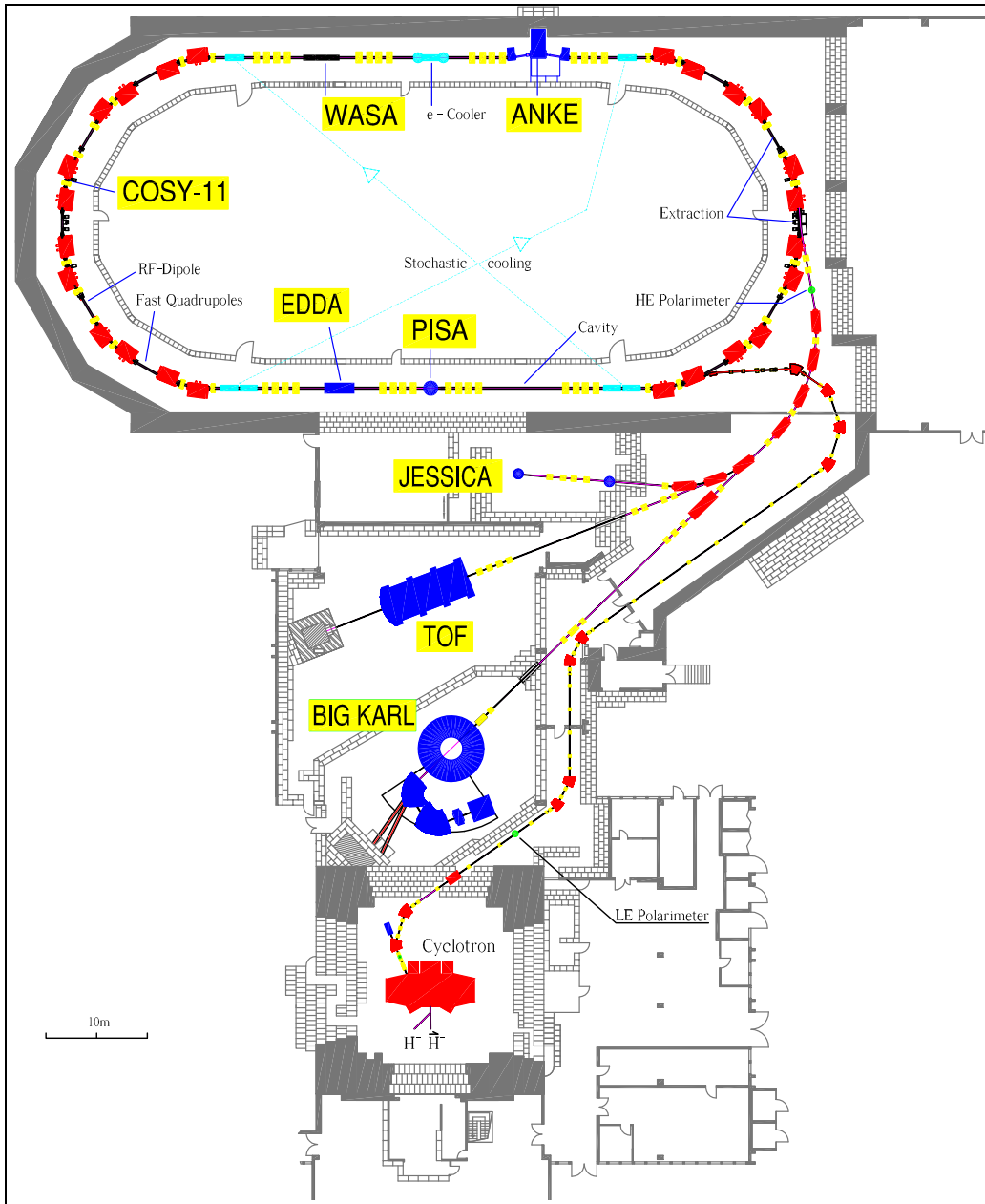


Figure 2: The accelerator complex with the cyclotron, the COSY ring and the experimental installations. The place of WASA is within one of the straight sections of COSY. For more details please visit <http://www.fz-juelich.de/ikp/cosy>.

2.2 The WASA detector

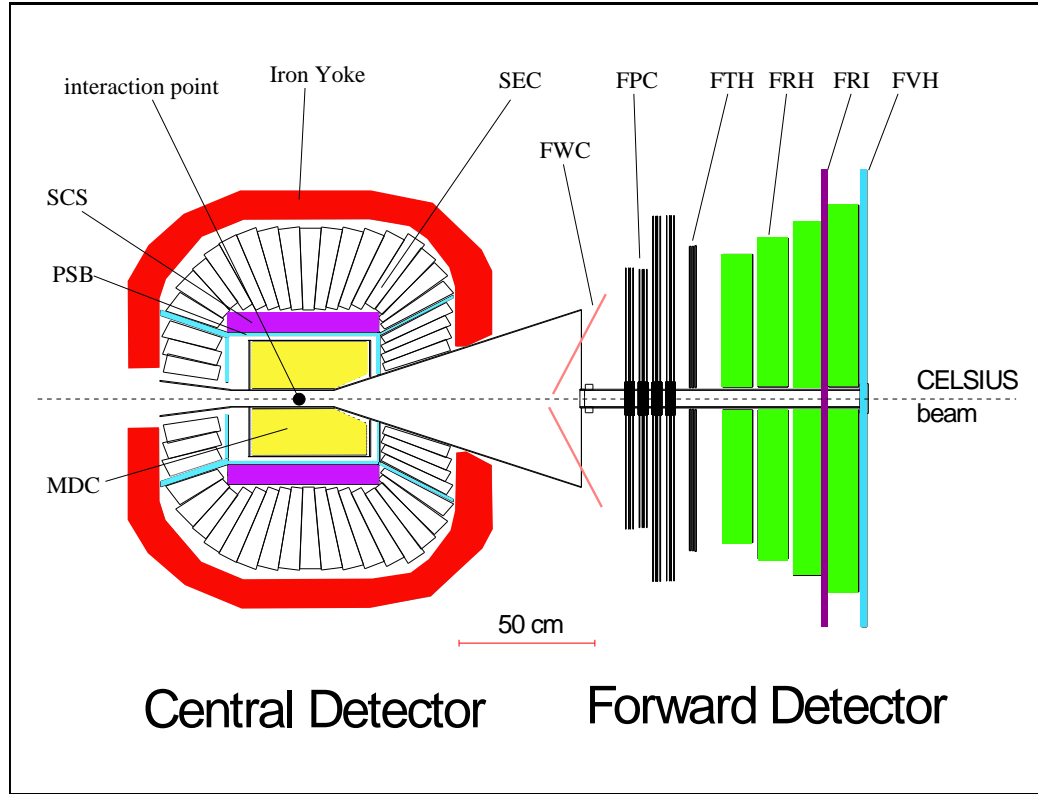


Figure 3: Cross section of the WASA detector as being used at CELSIUS. Beam comes from the left. The Central Detector (**CD**) build around the interaction point (at the left). The layers of the Forward Detector (**FD**) are shown on the right. Other symbols (MDC, PSB, FPC, ...) will be explained in text of the thesis.

As mentioned before the **WASA** detector – *Wide Angle Shower Apparatus* Fig. 3, was designed to study various decay modes of the η -meson. This is reflected in the detector setup. The η -mesons are produced in reactions of the type $pp \rightarrow pp\eta$. Due to the kinematics boost, the two protons are going into the forward direction, while the light decay products of the η are distributed into 4π .

In order to detect the protons, a ϕ -symmetric forward detector for $\theta \leq 18^\circ$ is installed. The particles are identified and reconstructed by means of dE measurement and track reconstruction using drift chambers. A trigger, which is set only on the forward detector, can be used to select events independently on the decay mode of the η -meson.

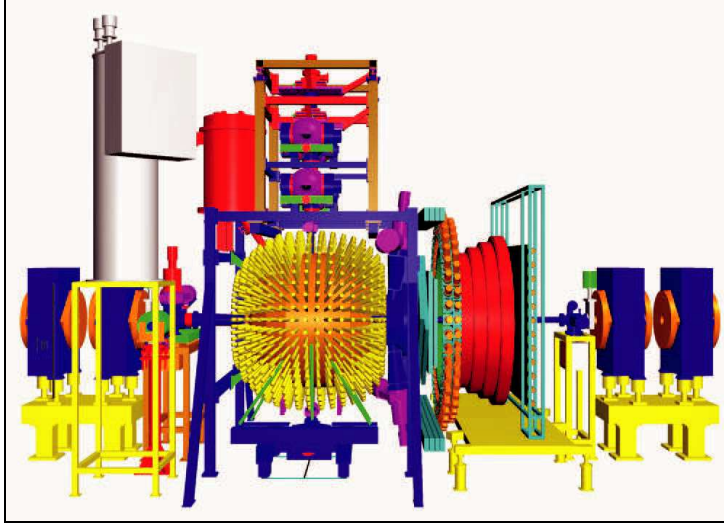


Figure 4: 3D View of the WASA detector[2].

Particles coming from meson decays are e^\pm, μ^\pm, π^\pm and γ , are detected in the central part of WASA ($\theta \geq 20^\circ$). Momentum reconstruction is done by tracking in a magnetic field and the energy of the particles is measured using an electromagnetic calorimeter. By including the central detector in the trigger also very rare decay modes can be studied while using a very high luminosity of up to $10^{32} \text{ cm}^{-2}\text{s}^{-1}$. A 3D view of the detector setup is presented in Fig. 4.

2.2.1 The Pellet Target

The pellet target system Fig. 5 was a special development for WASA. The "pellets" are frozen droplets of hydrogen or deuterium with a diameter between $25\mu\text{m}$ and $35\mu\text{m}$. The advantages of using pellet target compared with a standard internal gas target are the following:

- high target density, allows high luminosities necessary for studying rare decays
- thin tube delivery through the detector, 4π detection possible
- very good localized target, small probability of secondary interactions inside the target

The central part of the system is the pellet generator where a stream of liquid gas (hydrogen or deuterium) is broken into droplets by a vibrating

nozzle. The droplets freeze by evaporation into a first vacuum chamber forming a pellet beam. The beam enters a vacuum-injection capillary where it is collimated and is fed through a 2m long pipe into the scattering chamber Fig. 6. An effective beam thickness for hydrogen of 3×10^{15} atoms/cm² has been achieved with a beam diameter 2–4mm, a frequency of pellets 5–10kHz, and an average distance between the pellets of 9 – 20mm.

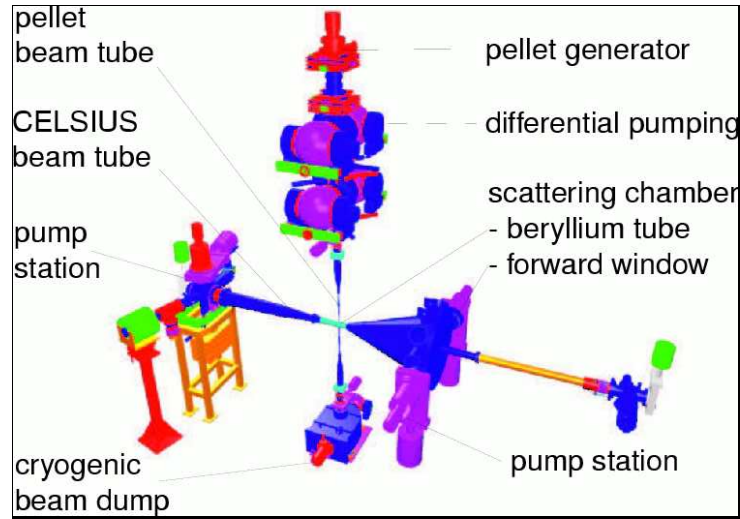


Figure 5: The Pellet Target system [2].

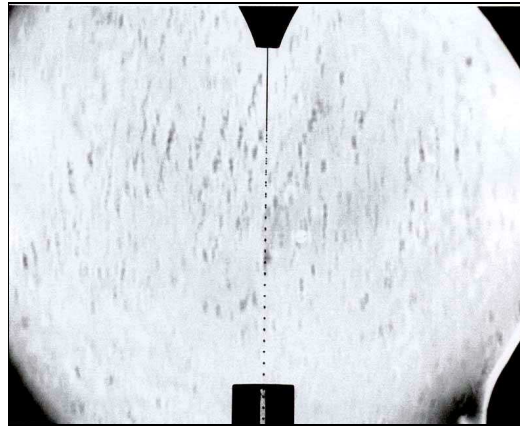


Figure 6: Photo of generated pellets [7].

2.2.2 The Forward Detector

The Forward Detector (FD) Fig. 3 tags meson production by measuring the energies (dE-E) and angles of forward scattered projectiles and charged recoil particles like protons and deuterons, also neutrons and charged pions. The produced mesons are then reconstructed using the missing mass technique. It covers angles from 3° to 18° . It consists of several layers of detectors described below:

- **FWC** The Forward Window Counters
The FWC is the first detector in the Forward Detector. It consists of 12 plastic scintillators of 5mm thickness. It is used to reduce the background from scattered particles originally from the beam pipe or the exit flange.
- **FPC** The Forward Proportional Chambers
The next detector is the FPC. It consists of 4 modules each containing 122 straw tubes detectors. The modules are rotated relatively to each other by 45° . The FPC is used as a precise tracking device.
- **FTH** The Forward Trigger Hodoscope
Close to FPC the FTH (“Jülich Quirl”) is installed. It consists of 3 layers of plastic scintillators, one with straight modules, two with bended ones. Each layer has a thickness of 5mm. It is used for a rough determination of the hit position on the higher level and as a starting value for the FPC analysis.
- **FRH** The Forward Range Hodoscope
The kinetic energy of the particles is measured by the FRH. It consists of 4 layers of cake-piece shaped plastic scintillators of 11cm thickness. There are 24 scintillators pro layer. It is also used for particle identification by the dE-E technique.
- **FRI** The Forward Range Interleaving Hodoscope
Between third and fourth layer of FRH two layers of plastic scintillators are installed (FRI). Each layer is made of 32 strips of 5.2mm thickness. The FRI is used to determine the scattering angles of neutrons.
- **FVH** The Forward Veto Hodoscope
The last layer of FD is FVH. It consists of 12 horizontally oriented scintillator strips with photomultipliers on both sides. The hit position is determined from the time differences of the signals. It is used to identify particles which are not stopped in the FRH.



2.2.3 The Central Detector

The Central Detector (CD) surrounds the interaction point and is constructed to identify energies and angles of the decay products of π^0 and η mesons, with close-to 4π acceptance. It consists of:

- **SCS** The Superconducting Solenoid
The SCS produces an axial magnetic field necessary for momentum reconstruction using the inner drift chambers. As superconductor NbTi/Cu is used cooled down by liquid He at 4.5K. The maximal central magnetic field is 1.3T. The return path for the field is done by a yoke made of 5 tons of pure iron with low carbon content.
- **MDC** The Mini Drift Chamber
The MDC is build around the beam pipe and it is used for momentum and vertex determination Fig. 7. It consists of 17 layers with in total 1738 straw tubes detectors. It covers scattering angles from 24° to 159° [3]. For the resolution refer to Tab. 1.

particle	p [MeV/c]	resolution $\Delta p/p$
electrons	20 – 600	< 1%
pions, muons	100 – 600	< 4%
protons	200 – 800	< 5%

Table 1: MDC resolution

- **PSB** The Plastic Scintillator Barrel
The PSB surrounds the MDC inside the SCS. It consists of 146 8mm thick strips that form a barrel like shape. It is used together with MDC and SEC, and acts as a dE-E and dE-momentum detector and as well as a veto for photons.
- **SEC** The Scintillator Electromagnetic Calorimeter
The SEC is the heart of the WASA detector and maybe the most important part. At CELSIUS it has been used to measure electrons and photons up to 800 MeV. However, using a different setting the energy range can be extended taking into account the higher energy available at COSY. It consists of 1012 CsI(Na) crystals shaped like a truncated pyramids Fig. 8. It covers angles from 20° to 169° and the crystals are placed in 24 layers along the beam Fig. 9. The lengths of the crystals vary from 30cm (central part), 25cm (forward part), 20cm (backward part). The forward part consists of 4 layers each 36 crystals,

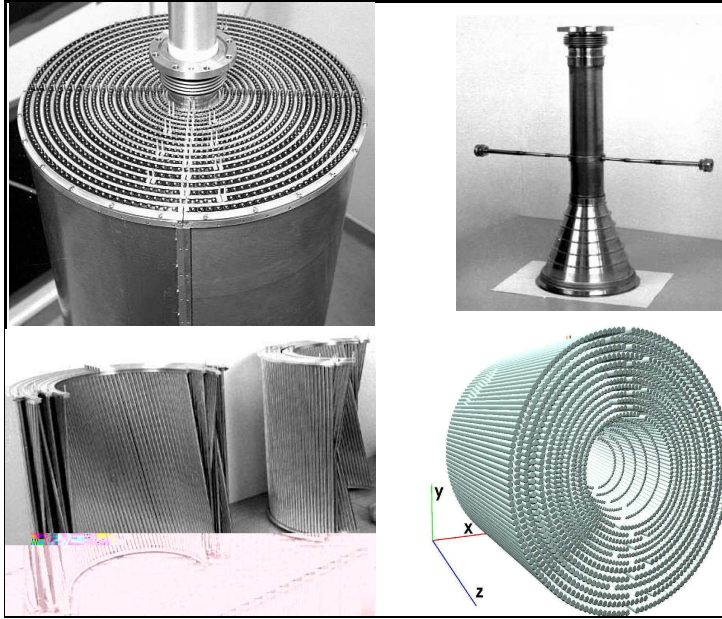


Figure 7: MDC and Be pipe. The fully assembled MDC inside Al-Be cylinder (upper left)[3].

covering the range of $20^\circ - 36^\circ$. The central part consists of 17 layers with 48 elements each, covering the range between $36^\circ - 150^\circ$, and the backward part with 3 layers, two with 24 crystals and one with 12. The geometrical distribution of the crystals can be seen in Fig. 10 and Fig. 11.

The calorimeter is composed of sodium doped CsI crystals. They are painted with transparent varnish for moisture protection and wrapped in $150\mu\text{m}$ teflon and $25\mu\text{m}$ aluminized mylar foil [5]. For more information refer to Tab. 2.

The advantages of using this type of material instead of CsI(Tl) are the following:

- emission peak at 420nm (CsI(Tl): 550nm) matches very well the spectral efficiency of the most commonly used PMT's
- the scintillation time is short
- much less afterglow
- much more radiation durability



Figure 8: CsI(Na) crystal fully equipped with light guide, PM tube and housing [5].

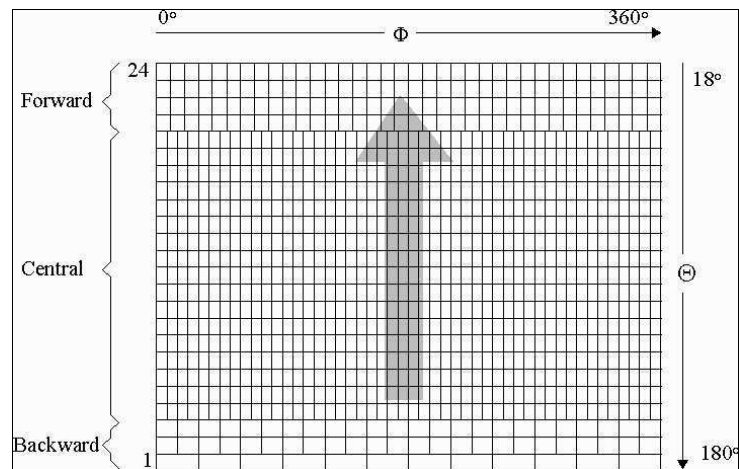


Figure 9: SEC planar map (arrow indicates beam direction) [2].

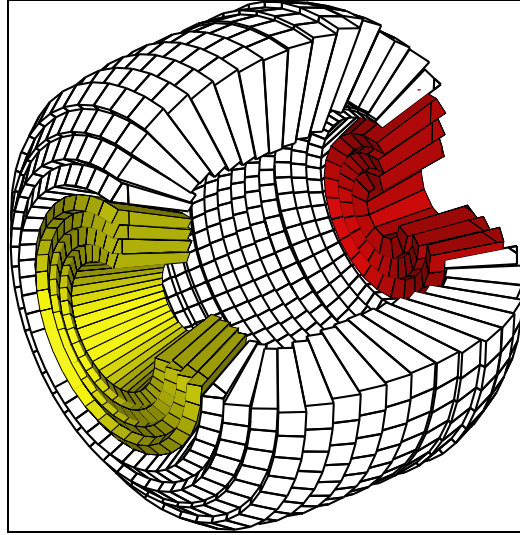


Figure 10: Schematic view of the calorimeter layout. It consists of the forward part (yellow, on the left), central part and the backward part (red, on the right) [2].

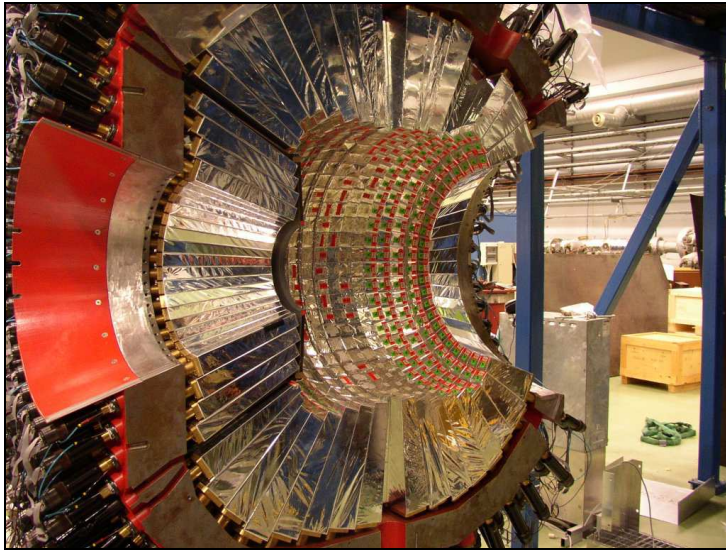


Figure 11: Photo of the SEC (forward to the left) [7].

amount of active material	16 X_0
geometric acceptance:	96%
polar angle:	20° – 169°
azimuthal angle:	0° – 180°
relative energy resolution: $Cs(137)662keV$	30% (FWHM)
maximal kinetic energy for stopping: pions/protons/deuterons	190/400/500MeV

Table 2: SEC parameters

Detailed comparison between several types of CsI crystals is presented in Tab. 3.

Scintillator (Activator)	CsI (Tl)	CsI (Na)	CsI (undoped)
Density [gcm^{-3}]	4.51	4.51	4.51
Hygroscopic	slightly	yes	slightly
Emission wavelength max [nm]	550	420	315
Lower Cut-off [nm]	320	300	260
Refractive index at emission max	1.79	1.84	1.95
Primary decay time [μs]	1.0	0.63	0.016
Light yield [10^3 photons/MeV]	52 – 56	38 – 44	2

Table 3: Properties of CsI scintillator crystals

2.3 Physics at WASA

The physics program at WASA will investigate symmetries and symmetry breaking as well as hadron structure and interactions. The planned experiments address the following topics: mixing of the scalar mesons $a_0/f_0(980)$, study of hyperon resonances, a_0^+ production, pentaquarks, isospin violation in $\vec{d}d \rightarrow \alpha\pi^0$ so it is permeated with newness.

However the most promising and intriguing problems, that maybe at WASA will be clarified, of the whole physics program are **rare and very rare decays of η and η' mesons**. Below I will try to outline the physics behind them.

The η and η' belong to the SU(3) lightest nonet Fig. 12 of the pseudoscalar mesons (0^-) [18].

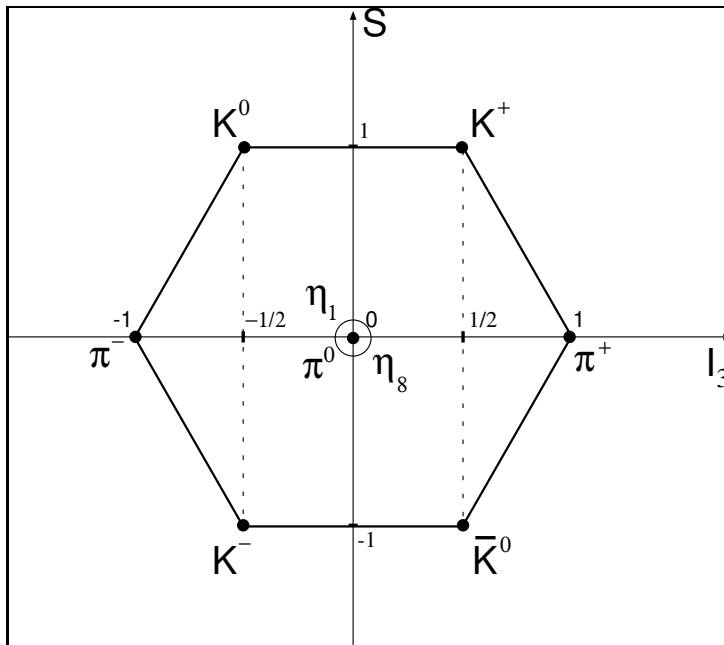


Figure 12: SU(3) nonet of pseudoscalar mesons.

We can write the pure SU(3) states as:

$$\left. \begin{aligned} \eta_8 &= \frac{1}{\sqrt{3}}(u\bar{u} + d\bar{d} + s\bar{s}) \\ \eta_1 &= \frac{1}{\sqrt{6}}(u\bar{u} + d\bar{d} - 2s\bar{s}) \\ \tilde{\pi}^0 &= \frac{1}{\sqrt{2}}(d\bar{d} - u\bar{u}) \end{aligned} \right\} \begin{array}{l} I = 0 \\ I = 1 \end{array}$$



States with the same quantum numbers can mix so $\tilde{\eta}$ and $\tilde{\eta}'$ are not pure SU(3) states only mixes of the singlet and octet states [10]:

$$\tilde{\eta} = \cos(\theta_p)\eta_8 - \sin(\theta_p)\eta_1$$

$$\tilde{\eta}' = \sin(\theta_p)\eta_8 + \cos(\theta_p)\eta_1$$

The mixing angle is rather small $\theta_p = -11.5^\circ$ [13] (different experimental approaches lead to different values between -10° and -20°). Mixing like this is allowed by the charge symmetry. But the situation seems not to be so simple, QCD Hamiltonian

$$H_{QCD} = H_{Color} + H_{Coulomb} + \underbrace{m_u u\bar{u} + m_d d\bar{d} + m_s s\bar{s}}_{H_m}$$

except the Color part H_{Color} contains also the Coulomb part $H_{Coulomb}$ and the part with quark masses H_m which mainly leads to non zero probability of transition between two different isospin states, so the transitions between the $\tilde{\eta}, \tilde{\eta}', \tilde{\pi}^0$ are possible. The physical mesons η, η', π^0 are not pure isospin states but only mixtures. Because of the high mass difference between the η and η' the strongest mixing effect would be observed for the pair $\pi^0 - \eta$. Lets now write the real meson states π^0, η :

$$\pi^0 = \cos(\theta_{\pi\eta})\tilde{\pi}^0 - \sin(\theta_{\pi\eta})\tilde{\eta}$$

$$\eta = \sin(\theta_{\pi\eta})\tilde{\pi}^0 + \cos(\theta_{\pi\eta})\tilde{\eta}$$

where $\theta_{\pi\eta}$ is the mixing angle between $\pi^0 - \eta$. The easiest way to determine the $\theta_{\pi\eta}$ is to measure the ratio of the widths between two decay modes of the η' meson $\Gamma(\eta' \rightarrow 3\pi)$ (not allowed by isospin symmetry) to $\Gamma(\eta' \rightarrow \eta 2\pi)$ (allowed by isospin symmetry) Tab. 5:

$$R_1 = \frac{\Gamma(\eta' \rightarrow \pi^0 \pi^0 \pi^0)}{\Gamma(\eta' \rightarrow \eta \pi^0 \pi^0)}$$

$$R_2 = \frac{\Gamma(\eta' \rightarrow \pi^0 \pi^+ \pi^-)}{\Gamma(\eta' \rightarrow \eta \pi^+ \pi^-)}$$

and then the $\theta_{\pi\eta}$ can be expressed [11]:

$$R_i = P_i \sin^2(\theta_{\pi\eta})$$

$$\sin(\theta_{\pi\eta}) = \frac{\sqrt{3}\Delta m}{4(m_s - \hat{m})}$$

wheres P_i is the phase-space factor, $\Delta m = m_d - m_u$, $\hat{m} = (m_d + m_u)/2$.



Not only these four decay modes will be investigated, thanks to the high production rate Tab. 4, WASA opens possibility to study really **very rare** processes Tab. 5. Lots of these reaction will be measured first time in the world. For more details look at [2].

$L = 1*10^{32}$ [cm ⁻² s ⁻¹]	$pp \rightarrow pp \eta$	$pp \rightarrow pp \eta'$
T _{beam} [GeV]	1.5	2.54
P _{beam} [GeV]	2.25	3.35
Q [MeV]	94	45
σ [μ b]	25	0.3
Rate [1/s]	2500	30

Table 4: Production rates at WASA

Decay	BR	Existing data events in the world	WASA@COSY events per day
$\eta' \rightarrow \pi^0 \pi^0 \eta$	20.9%	5400	14500
$\eta' \rightarrow \pi^0 \pi^0 \pi^0$	1.56*10 ⁻³	130	145
$\eta' \rightarrow \pi^+ \pi^- \eta$	44.3%	8200	18000
$\eta' \rightarrow \pi^+ \pi^- \pi^0$	< 5.%	-	85
$\eta' \rightarrow \rho^0 \gamma$	29.5%	9550	44000
$\eta' \rightarrow \omega \gamma$	3.03%	160	1200
$\eta' \rightarrow \gamma \gamma$	2.12%	2667	17100
$\eta' \rightarrow \mu^+ \mu^- \gamma$	1.04*10 ⁻⁴	33	15
$\eta' \rightarrow e^+ e^- \gamma$	< 9.*10 ⁻⁴	-	45
$\eta \rightarrow e^+ e^- \pi^+ \pi^-$	4.*10 ⁻⁴	5	7000
$\eta \rightarrow e^+ e^- e^+ e^-$	< 6.9*10 ⁻⁵	-	450
$\eta \rightarrow e^+ e^-$	< 7.7*10 ⁻⁵	-	1/6
$\eta \rightarrow \pi^0 e^+ e^-$	< 4.*10 ⁻⁵	-	1/15 – 1/2

Table 5: Decays of η and η' at WASA

3 Physics of Calorimetry

Calorimeters are devices used to measure energy of electrons, photons and hadrons. In order to do this they are usually build as a block of instrumented material in which the particles are fully absorbed and their energy is transformed to the measurable quantity. The calorimeters could be divided in general into hadronic and electromagnetic calorimeters. Hadronic calorimeters are used to measure hadrons through their strong and electromagnetic interactions. Due to involvement of nucleon (hadronic) interactions the energy deposit is widely spread and the resolution is quite bad (typically 30 – 50%). Electromagnetic calorimeters are used to measure energy and position of electrons(positrons) and photons by means of their electromagnetic interactions (bremsstrahlung, pair production) with matter. I will concentrate on the latter ones i.e. *the electromagnetic calorimeters*. To understand how they work first the electromagnetic interactions will be investigate.

3.1 Some definitions

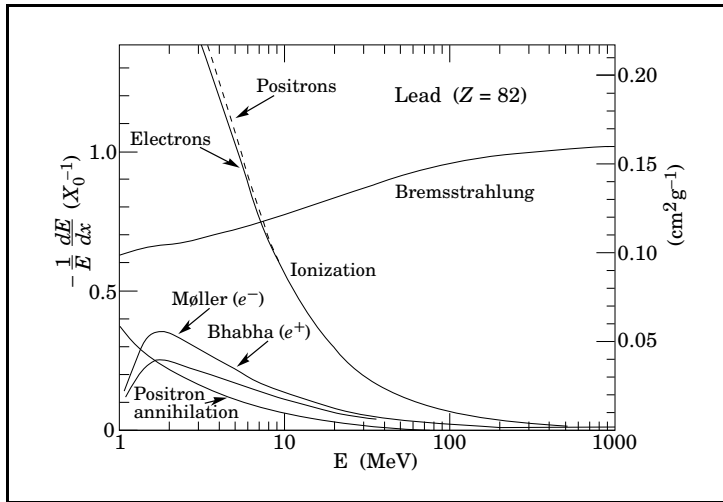


Figure 13: Energy loss of electrons per radiation length in Pb as a function of energy [13].

Electrons and photons interact with matter over today good understood QED processes, so the description of them is possible using simple empirical approach. There are two main regimes that govern their interactions Fig. 13 shows the fractional energy loss of electrons in lead and Fig. 14 shows photon interaction cross section. As can be seen for energies larger than $\sim 10\text{MeV}$

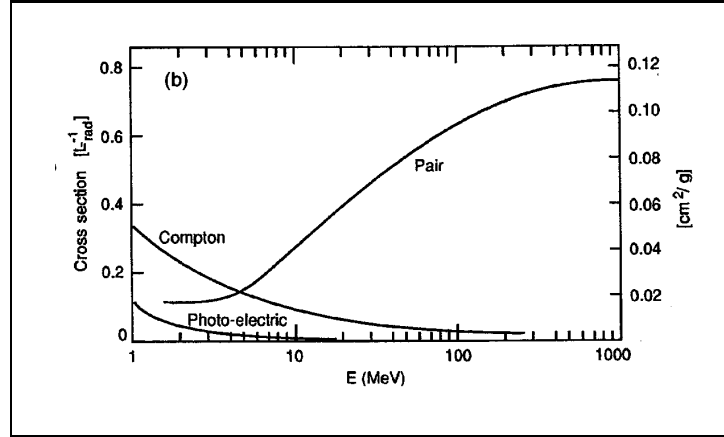


Figure 14: Photon interaction cross section in Pb as a function of energy [14].

photons mainly interact by pair production, while electrons lose their energy mostly by bremsstrahlung. For energies $> 1\text{GeV}$ these processes become energy independent. In the lower energy regime, for photons Compton and photo-electric effect dominate, for electrons however ionization rises, traversing electron or positron in matter undergoes collisions with molecules and atoms. It is considered as a ionization when energy loss per collision is below 0.255MeV . Although other processes also contribute: Bhabha scattering and annihilation of positrons and Möller scattering for electrons. The consequence of this behaviour is that the sufficiently high energetic photons or electrons interact with material producing secondary electrons by pair production and photons by bremsstrahlung. These secondary particles produce again further particles giving rise for an *electromagnetic shower* Fig. 15. This process continues as long as the energy is high enough to produce other particles. The limit is indicated by so called *critical energy* E_c (to be defined later).

The proper scale for the shower process (expansion description) is the *radiation length* X_0 , usually given in gcm^{-2} [13]. That is defined as:

- mean distance over which the electron will lose $1/e$ of its initial energy by bremsstrahlung

$$\langle E(x) \rangle = E_0 \exp[-x/X_0], \quad (1)$$

- $7/9$ of the mean distance over which the photon beam will lose $1/e$ of its intensity

$$\langle I(x) \rangle = I_0 \exp[-x7/(9X_0)]. \quad (2)$$

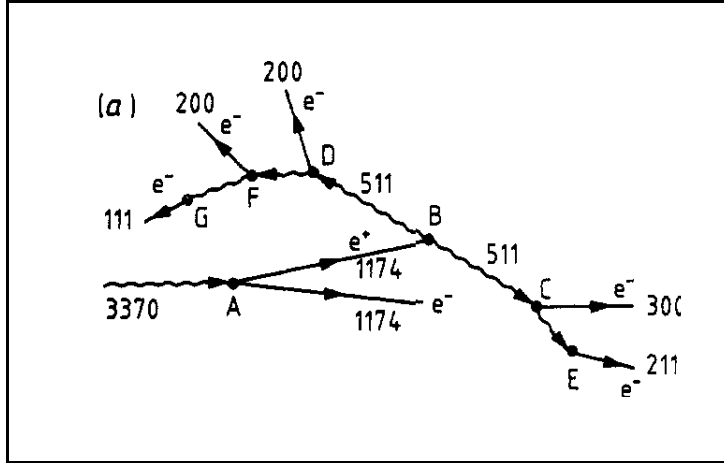


Figure 15: Possible shower development induced by few MeV gamma, the energies of e^\pm , γ are given in keV. Following processes are indicated: A - conversion to e^+e^- pair, B - annihilation of e^+ into two gammas, C, D, F - Compton scattering, E, G - photoelectric effect [17].

The *radiation length* depends on the type of material, and can be expressed as [13]:

$$X_0 = \frac{716.4 \text{ gcm}^{-2} A}{Z(Z+1) \ln(287/\sqrt{Z})}, \quad (3)$$

where Z - atomic number of the material, A - weight number of the material.

In case of compound material it can be approximated by:

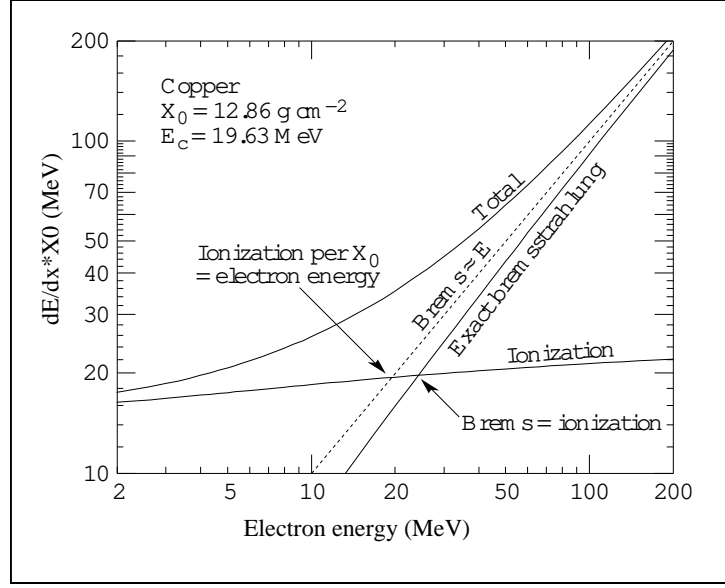
$$1/X_0 = \sum w_j/X_j, \quad (4)$$

where w_j - fraction by weight of the j -th element, X_j - radiation length of the j -th element.

The *critical energy* E_c mentioned above is not so clear-cut defined. There are two definitions used Fig. 16:

- *critical energy* is the energy at which ionization energy loss of electron is equal energy loss by bremsstrahlung

$$\left. \frac{dE}{dx} \right|_{\text{brems}} = \left. \frac{dE}{dx} \right|_{\text{ioniz}} \quad (5)$$

Figure 16: Two definitions of the critical energy E_c [13].

- *critical energy* is the energy at which ionization energy loss equals electron energy E divided by radiation length X_0

$$\left. \frac{dE}{dx} \right|_{ioniz} = \frac{E}{X_0}, \quad (6)$$

this is the same as the first definition Eq. 5 with approximation

$$\left. \frac{dE}{dx} \right|_{brems} \approx \frac{E}{X_0}. \quad (7)$$

As shown in Eq. 1 and Eq. 2 the scale for electromagnetic cascade developed by incident photon or electron is the same and is expressed by radiation length X_0 . So now we can describe in proper way the dimensions of the cascade.

The *mean longitudinal shower profiles* of energy deposits Fig. 17 are well described by a gamma distribution:

$$\frac{dE}{dt} = E_0 \frac{b^a t^{a-1} e^{-bt}}{\Gamma(a)}, \quad (8)$$

where E_0 is the incident particle energy, a, b are parameters depending on the type of incident particle (e^\pm, γ) and t is depth in the material in terms

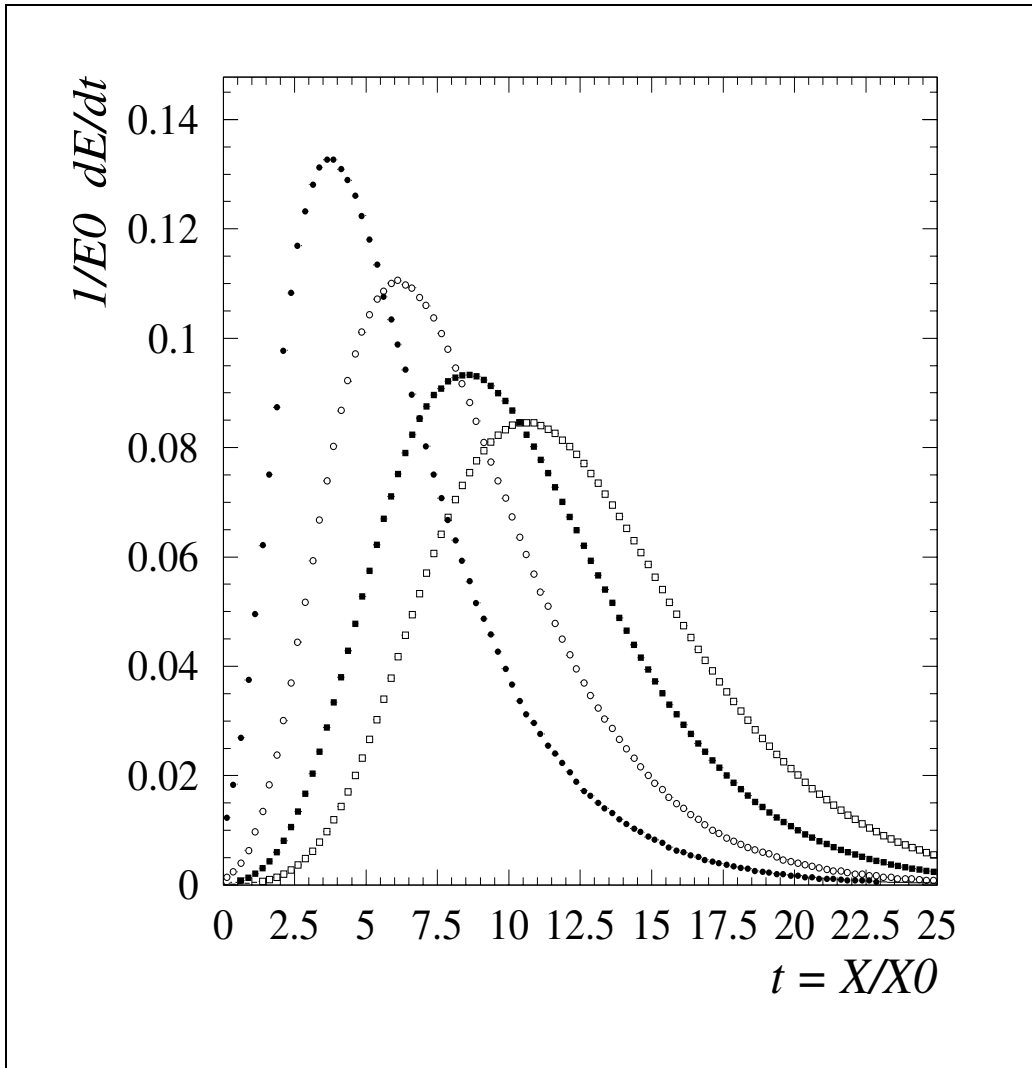


Figure 17: Longitudinal shower profiles simulated in PbWO_3 in dependence of the material thickness in radiation length, for e^- energy 1GeV, 10GeV, 100GeV, 1TeV from left to right [14].

of radiation length. The maximum of this distribution is located at $t_{max} = (a - 1)/b$ which is usually estimated as:

$$t_{max} = \ln \left(\frac{E_0}{E_c} \right) + t_0, \quad (9)$$

where t_0 depends on type of the particle and is $-0.5(0.5)$ for an electron(photon) induced cascade. (E_c is critical energy defined earlier.)

It can be seen in Eq. 9 that the expansion of the electromagnetic cascades is logarithmic and in consequence the detector thickness needed to absorb the energy scales the same way. The thickness that contains the 95% of the shower energy, for material with atomic number Z , can be derived as:

$$t_{95\%} = t_{max} + 0.08Z + 9.6. \quad (10)$$

The transverse development of the shower is mainly caused by multiple scattering of e^\pm away from the shower axis. Bremsstrahlung photons of these e^\pm also contribute to the cascade spread. The *transverse profile of the shower* is usually characterised by *the Molière radius* R_M . Transverse size integrated over full shower depth, representing the mean lateral deflection of electrons after traversing one radiation length and it is expressed as:

$$R_M = E_s \frac{X_0}{E_c}, \quad (11)$$

with E_s scale energy $\sqrt{4\pi/\alpha} m_e c^2 \approx 21\text{MeV}$ (here α Fine structure constant) and E_c critical energy from Eq. 6. On the average in a cylinder of $\sim 1R_M$ radius 90% of shower energy is contained. The transverse size of the electromagnetic shower is energy independent as can be seen on the Fig. 18.

3.2 The electromagnetic calorimeter itself

The principle of energy measurement with an electromagnetic calorimeter is that the energy deposited in calorimeter medium by charged particle of the cascade is proportional to the energy of the incident particle. Therefore the total track length of the cascade T_0 (sum of all ionization tracks in cascade) is proportional to

$$T_0 \sim X_0 \frac{E_0}{E_c}, \quad (12)$$

where E_0/E_c – number of particles in the cascade. So the measurement of the signal produced by particles in the shower gives estimation of the incident particle energy.



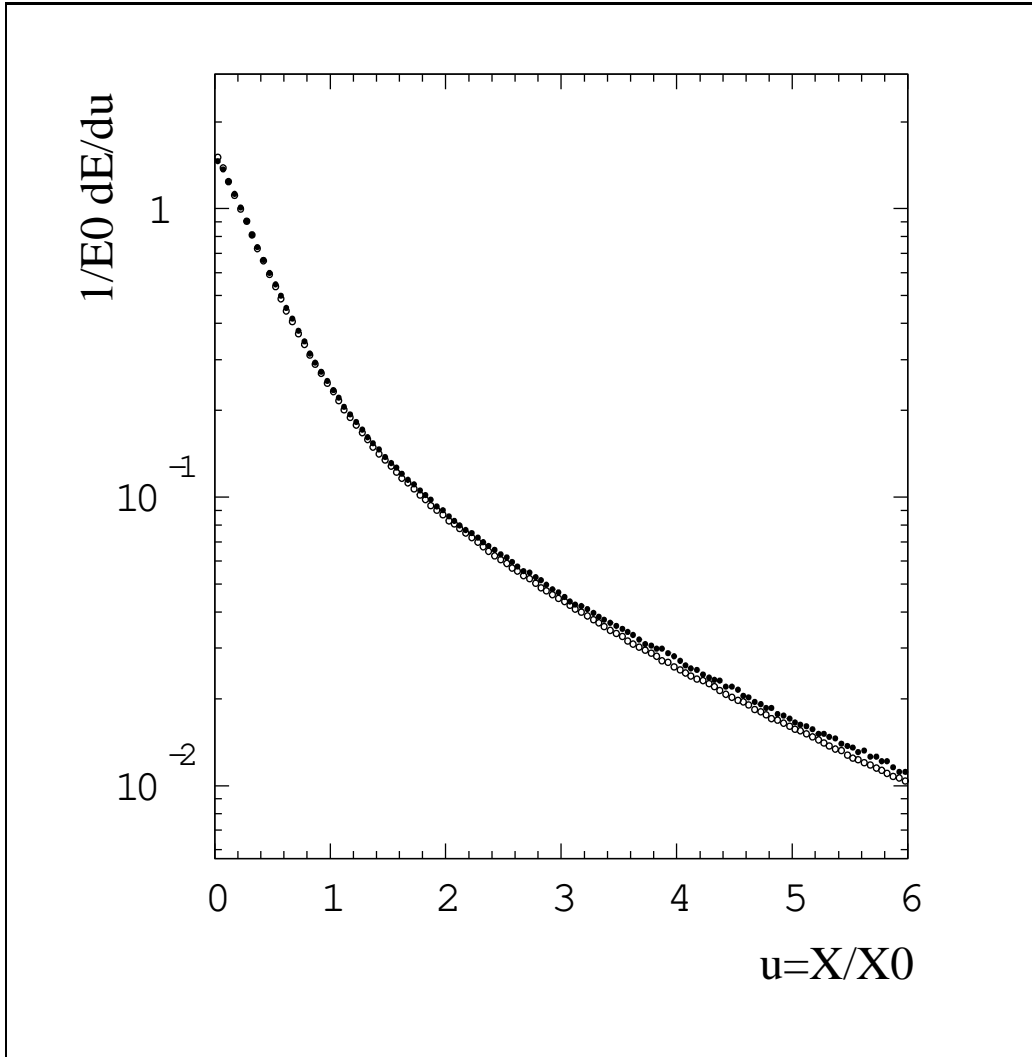


Figure 18: Transverse shower profiles simulated in PbWO₃ in dependence of the transverse distance from the shower axis in radiation length's for e^- energy 1 GeV(closed circles) and 1 TeV(open circles) [15].

As an example of the calorimeter let us consider the electromagnetic calorimeter of the WASA detector setup(section 2.2.3 on page 14). It is a scintillation calorimeter with inorganic CsI(Na) crystals. The mechanism of scintillation is related to the crystalic structure of the material. Charged particles are producing electron-hole pairs in the conduction and valence bands of the medium. When electrons return to the valence band the photons are emitted. The responce time and the wave length of the photons depends on the gap between the valence and conduction band and on the electron transport in the lattice structure. To increase the light yield and the response time crystals are usually doped with some amounts of inpurities, in our example Na, that create additional activation sites in gap between the bands thus increasing the probability of light emission.

So in this case the amount of light, emitted by scintillation process, induced by electromagnetic shower and collected by photomultiplier is proportional to the energy of incident particle.

The *energy resolution* of ideal calorimeter (infinite size, homogeneous response) is govern mainly by track length fluctuations. The shower development, as known, is a stochastic process, thus the energy resolution:

$$\sigma(E) \sim \sqrt{T_0}, \quad (13)$$

using Eq. 12 we can derive:

$$\frac{\sigma(E)}{E} \sim \frac{1}{\sqrt{T_0}} \sim \frac{1}{\sqrt{E_0}}. \quad (14)$$

The energy resolution of a realistic calorimeter is not so simple defined. Usually it is written the following way:

$$\frac{\sigma(E)}{E} = \frac{a}{\sqrt{E}} \oplus \frac{b}{E} \oplus c, \quad (15)$$

where \oplus – addition in quadrature.

The three terms in Eq. 15 contribute into resolution:

- *the stochastic term* a/\sqrt{E}

This term comes from the internal fluctuations of shower development, as described above. Typical values for this contribution are on the level of few percents.

- *the noise term* b/E

This term comes from electronic noise of readout chain and depends on features of the circuit. This contribution to energy resolution increase with decreasing energy and may be dominant for energies below few GeV.



- the constant term c

This term includes effects that do not depend on the incident energy of the particle, such as instrumental effects like imperfection of mechanical structure, temperature gradients, detector aging, radiation damage etc. All these effects cause nonconformities of the response signal, thus smearing measured energy. Usually this term should be kept in orders of 1%.

Sample energy resolution curves fitted by Eq. 15 are presented in Fig. 19 for three different scintillator crystals. The parameters of fit are for CeF_3 $a = 2.17\%$, $c = 2.7\%$; for PbWO_4 $a = 1.41\%$, $c = 0.9\%$ and for BaF_2 TAPS spectrometer $a = 0.59\%$, $c = 1.9\%$.

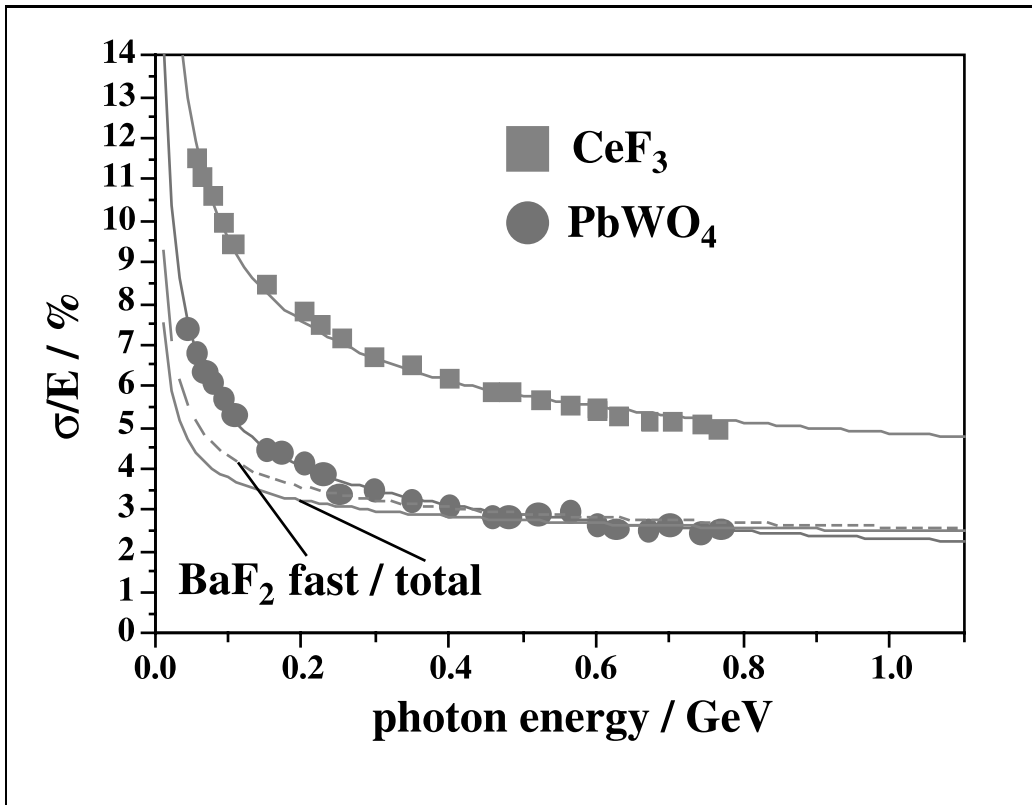


Figure 19: Energy resolution of CeF_3 and PbWO_4 crystals in comparison with BaF_2 scintillators of the TAPS spectrometer [16].

4 Measurements of the WASA calorimeter

The aim of these measurements was to check the Electromagnetic Calorimeter of WASA after the transport to IKP and to find broken elements as well as those with bad performance. In addition the test results will be used for the relative energy calibration of the CsI(Na) crystals. All channels were checked using source providing 4.4MeV photons (section 4.3). The results were then compared to cosmics measurements which have been performed for few channels (section 4.4).

4.1 Electronics setup

The electronics and readout system used for the test measurements is shown in Fig. 21. In all measurements only one crystal was readout at once. The signals from the crystal Fig. 22 were then amplified by a factor of 100 [ps 776] and split into two branches. One branch was used to construct the trigger: the signal was connected to the discriminator [LeCroy 821] in order to adjust the minimum signal level at which the signal should be sampled. The (logical) output of the discriminator was used to create a $12.2\mu\text{s}$ long gate [dual timer C.A.E.N. N93B], which defines the time window, in which FlashADC samples the input signal. The second line from the amplifier was delayed by 600ns (in order to compensate the time for trigger generation and to start sampling well ahead of the signal). The used Flash ADC [SIS 3300] had a frequency of 100 MHz. After digitization the data were sent via crate controller to the computer by a special PCI card and read using data aquisition delivered by ZEL¹(EMS system). The data were written to disk. During the measurements the spectra were monitored on-line using the RootSorter[20] analysis software.

¹<http://www.fz-juelich.de/zel>



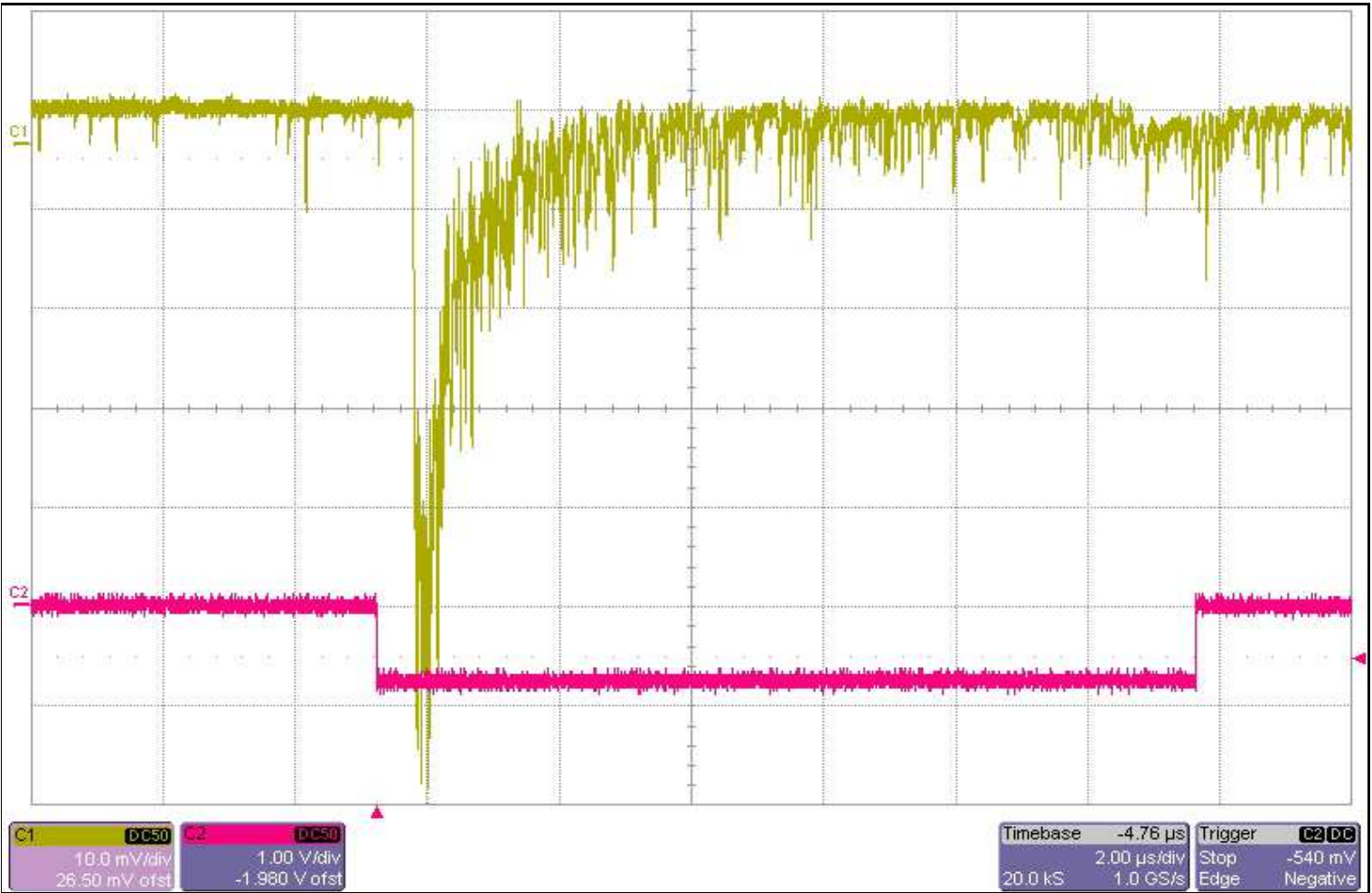


Figure 20: Raw FlashADC signal from CsI crystal as seen on the oscilloscope. The time gate used is also presented (lower line).

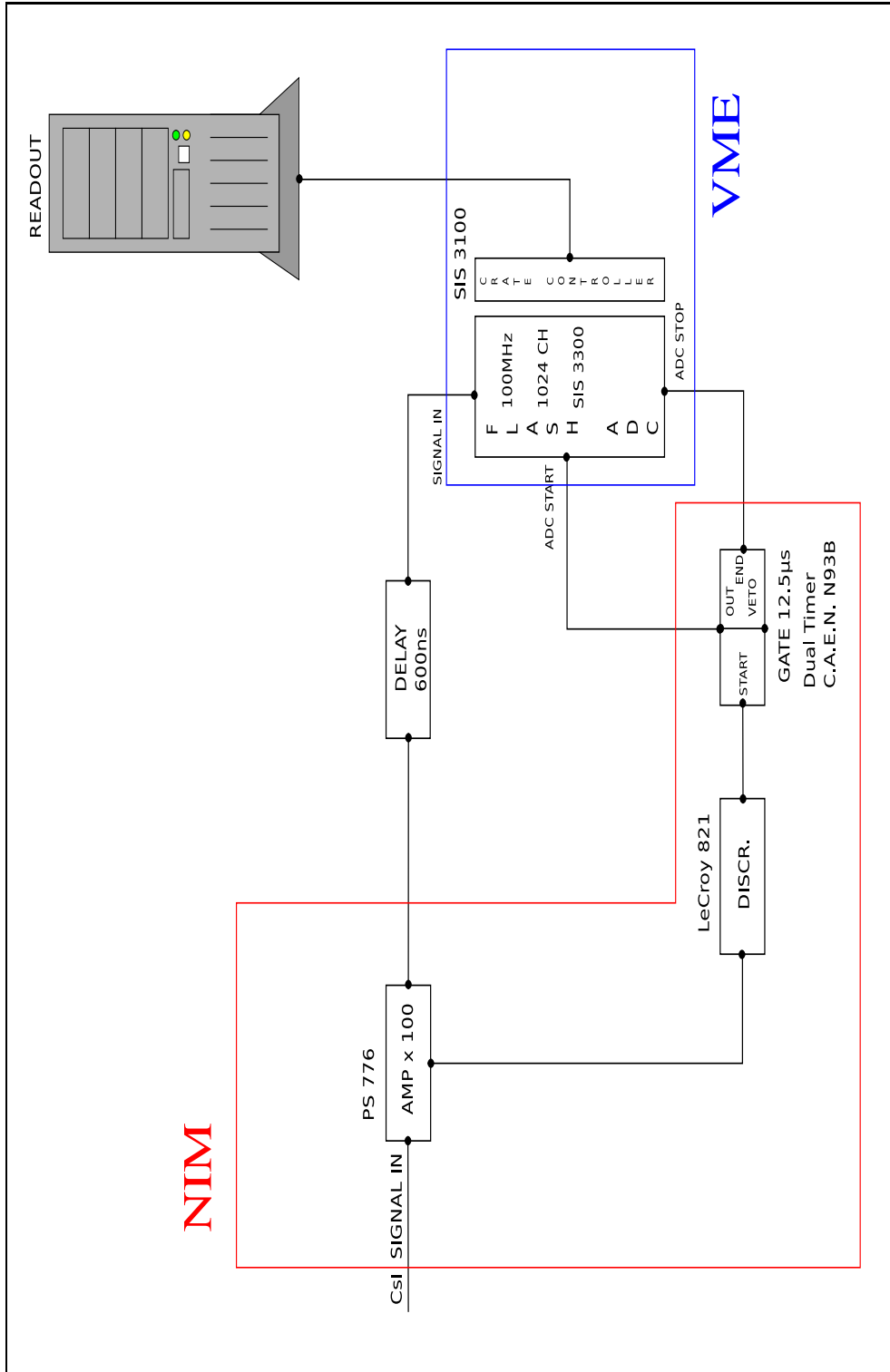


Figure 21: Electronics setup for measurements

4.2 General Analysis

The data were analysed event-by-event. For each sampled pulse Fig. 22 the zero level was computed as a mean value of first 30 channels and subtracted from the original signal. The integration gate was selected by comparing different spectra using various integration gates Fig. 23. The signal to background ratio was taken into account as well as the resolution and the optimal gate was selected. The further analysis was then based on the calculation of the normalized integral within this gate (channel 30 to 200).

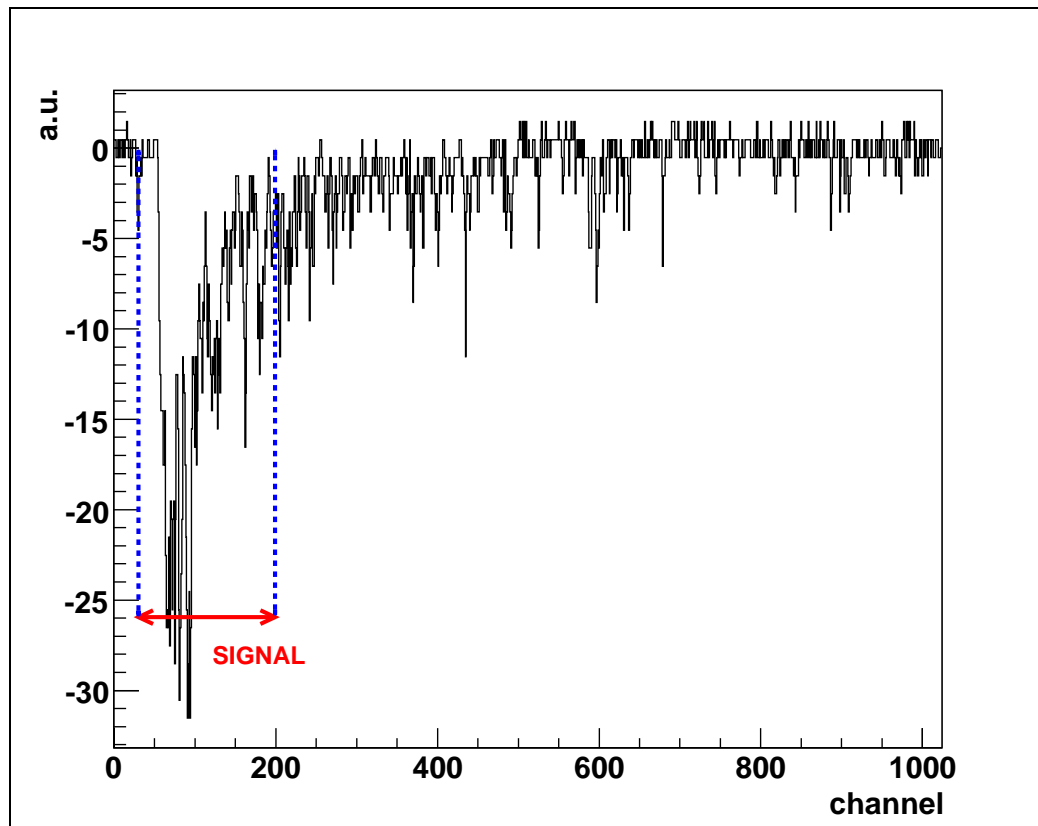


Figure 22: Sample CsI signal with subtracted ground level. The finally selected integration gate marked channel (30 – 200).

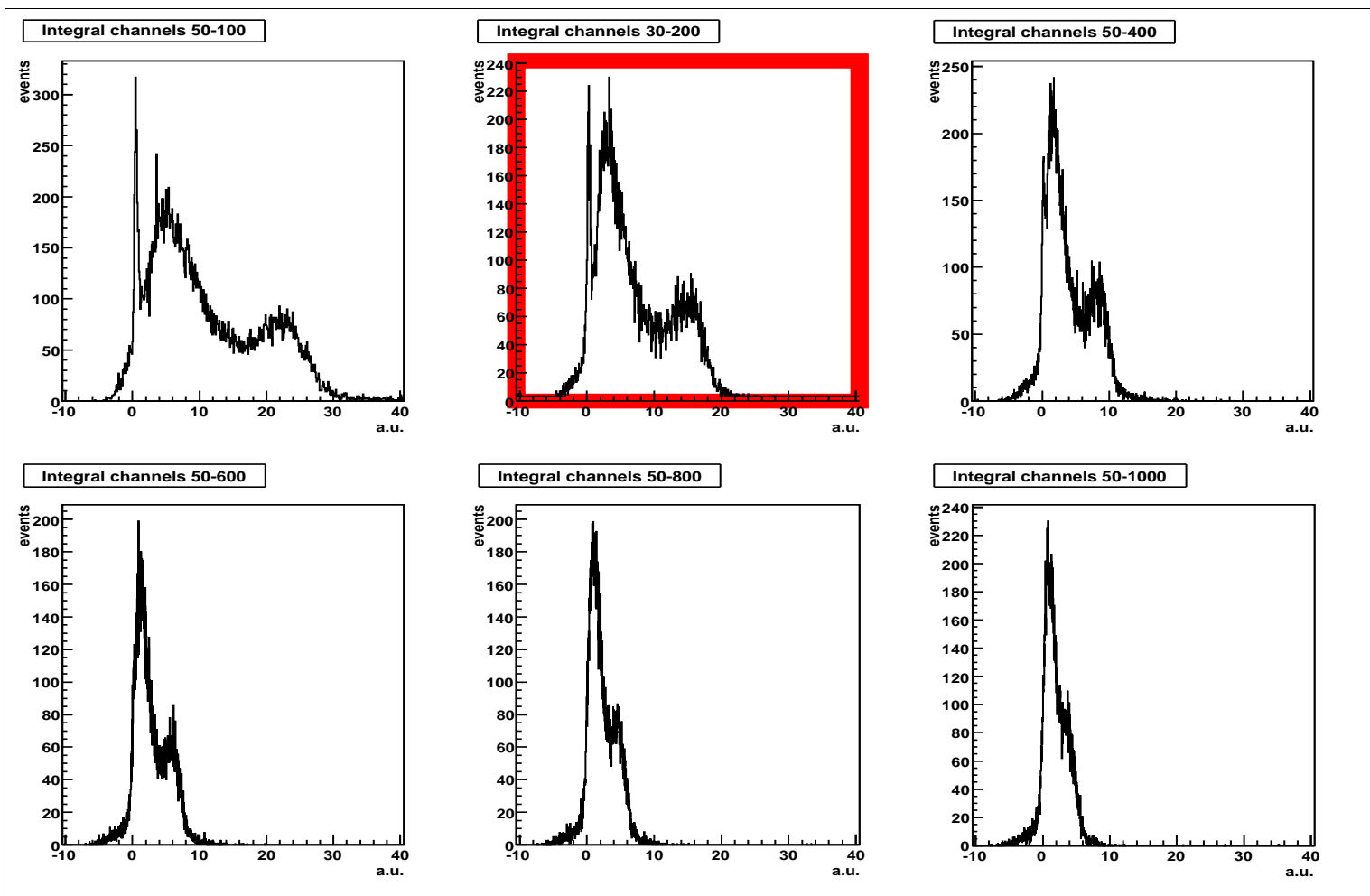


Figure 23: Integrated pulses for different integration gates. Selected gate is marked.



4.3 Source measurements

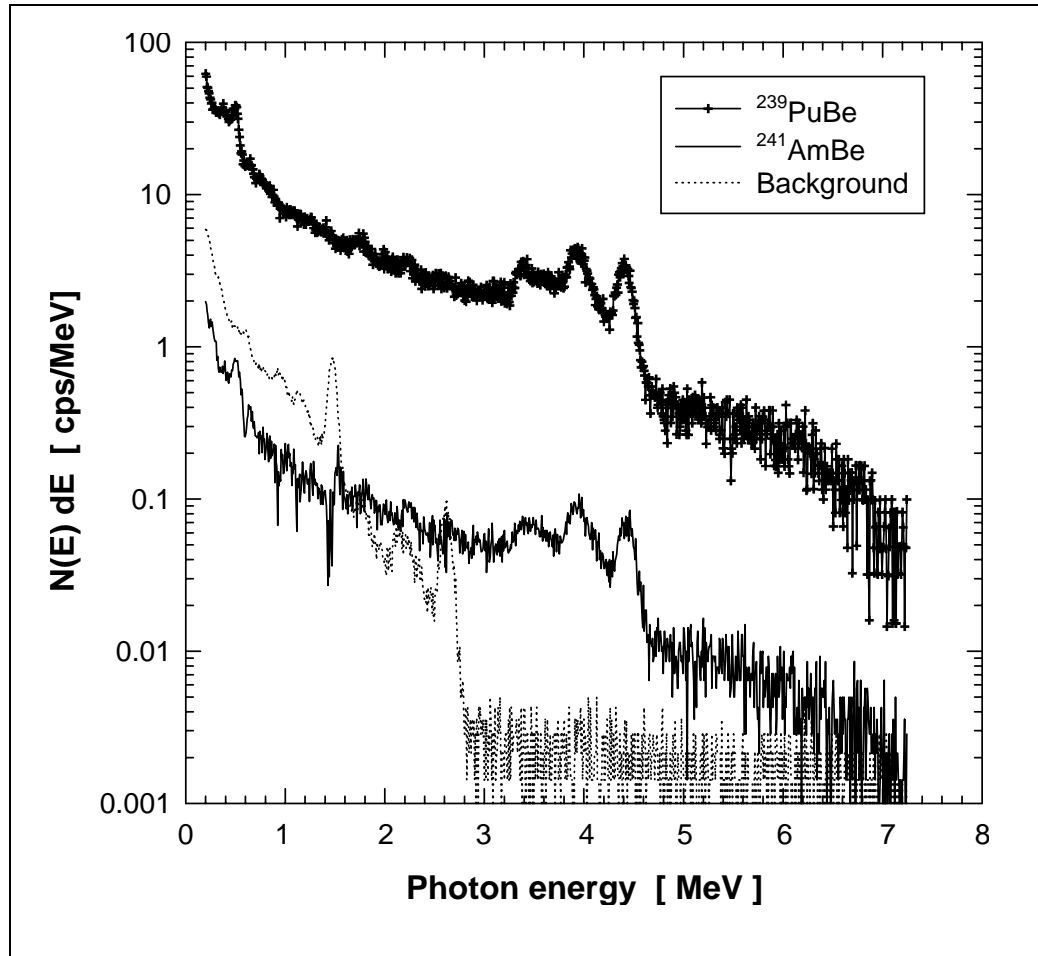


Figure 24: Gamma ray spectra of $^{239}\text{PuBe}$ source (upper spectrum) and $^{241}\text{AmBe}$ source (lower spectrum) measured using Na(Tl) scintillator [9].

The measurements of individual crystals were done with $^{241}\text{AmBe}$ radioactive source, see Fig. 24, which emits 4.4MeV photons. The experimental setup is shown in Fig. 25 and Fig. 26. The source was pushed as close as possible to the surface of the CsI crystals. The electronics setup was as described in section 4.1. The data first were treated as explained in section 4.2, the spectrum Fig. 27 is a result of it. The analysis using ROOT[19] was performed, by fitting two functions to the spectra, one describing the background(as exponential) and one describing the signal(as a Gauss function). The exponential background is probably a consequence of electronic

noise. Using this technique the peak position and the width of the signal was extracted from the data for each tested module. A typical spectrum with fitted background and signal function is shown in Fig. 28.

The peak position of the signal was plotted versus photomultiplier high voltage Fig. 29 to check working conditions. Corrections were applied to high voltage setting of the modules to adjust the gain to the same working level. In total around 100 channels were corrected, the resulting distribution is shown in Fig. 30. The full results from performed tests, for each channel, can be find in the Appendix A on page 59.

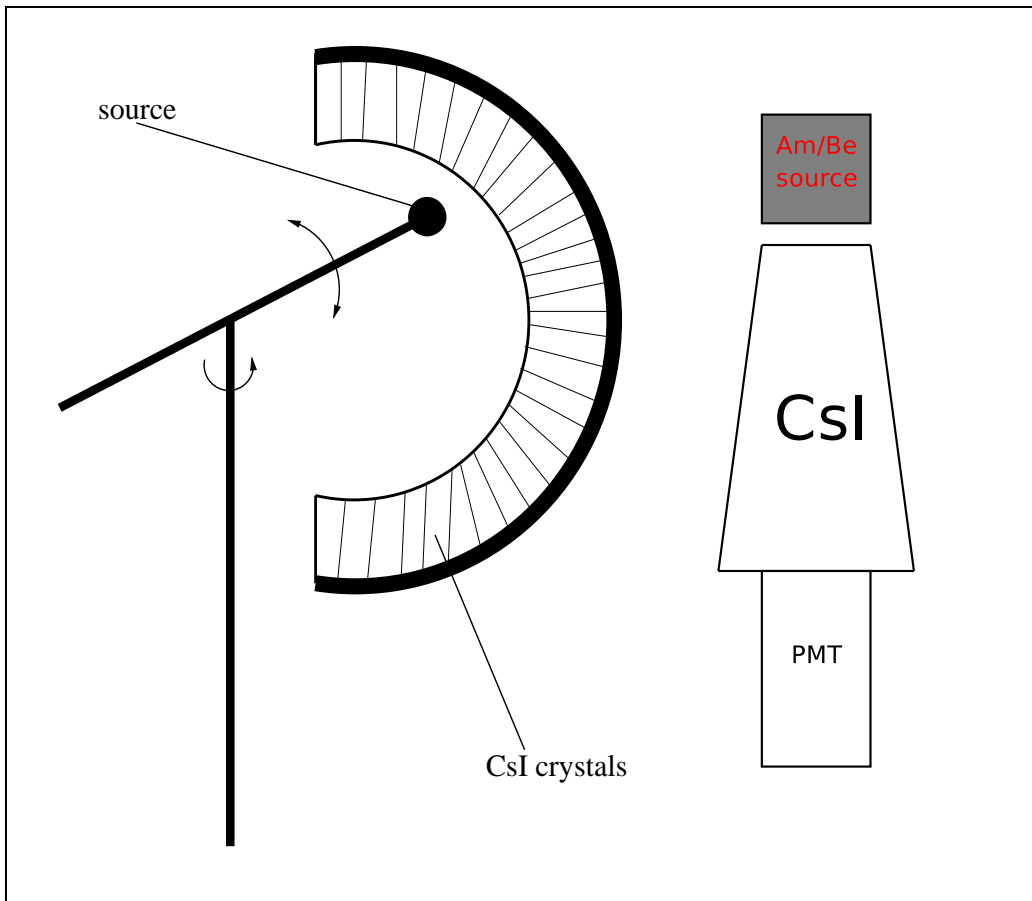


Figure 25: Setup for source measurements.

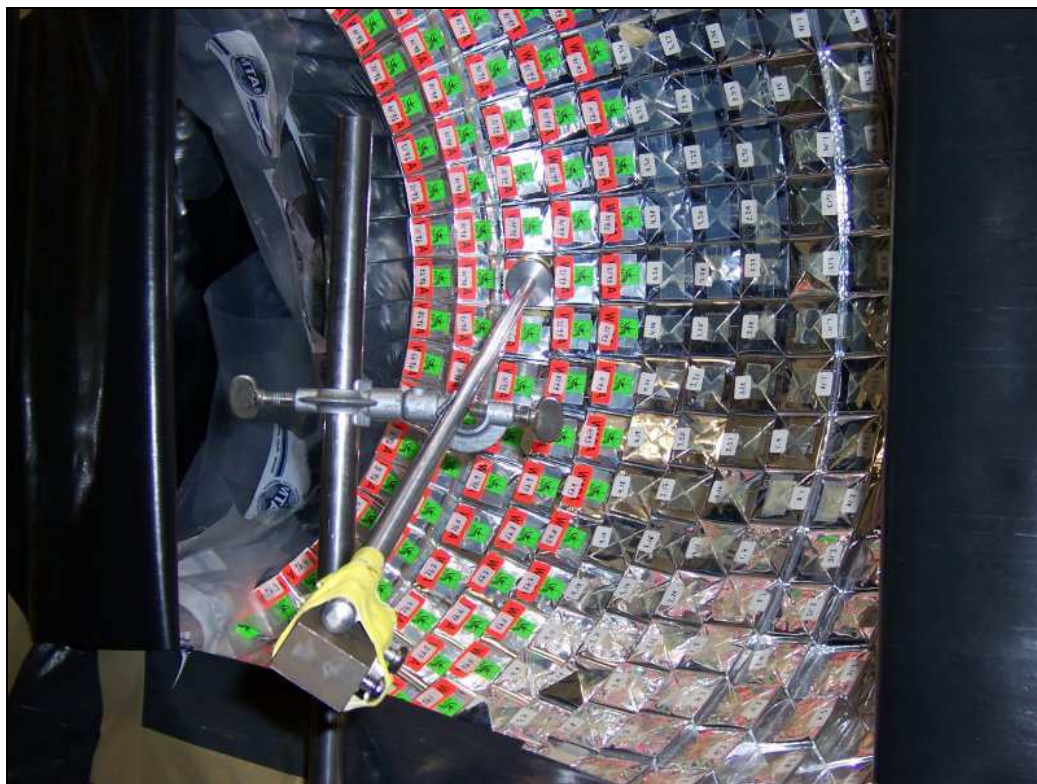


Figure 26: Photo of setup for source measurements.

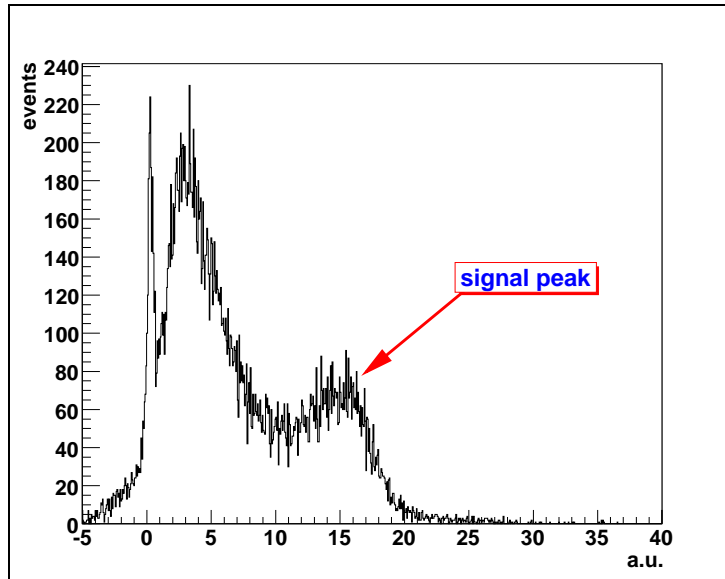


Figure 27: A sample ADC spectrum. The photon peak is indicated.

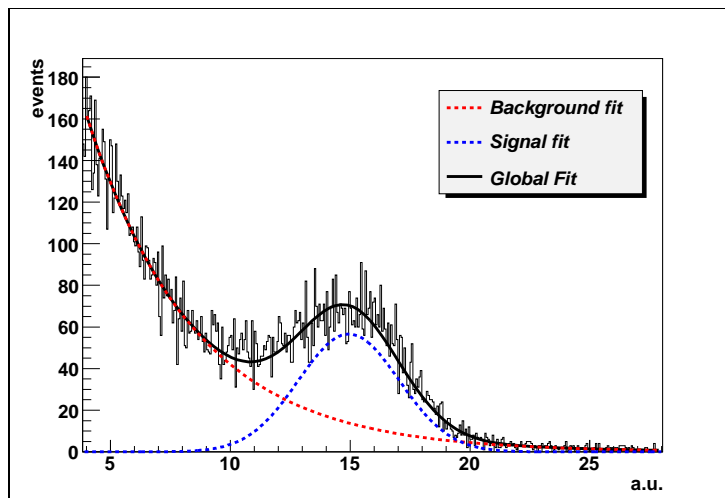


Figure 28: One fitted ADC spectrum.

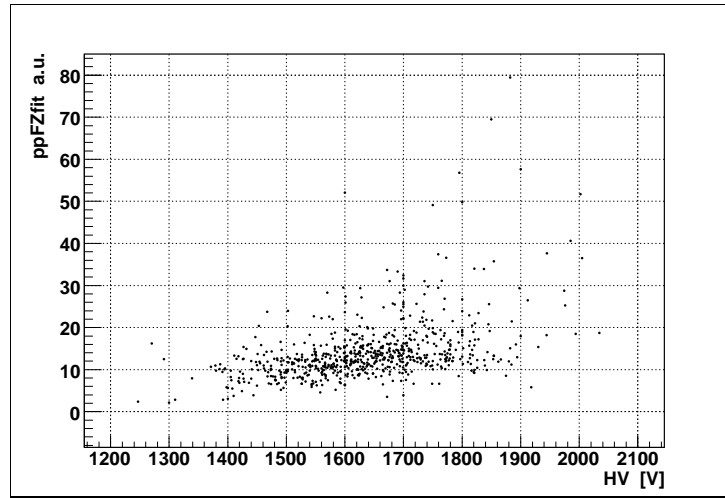


Figure 29: Measured peak position of the crystals versus high voltage.

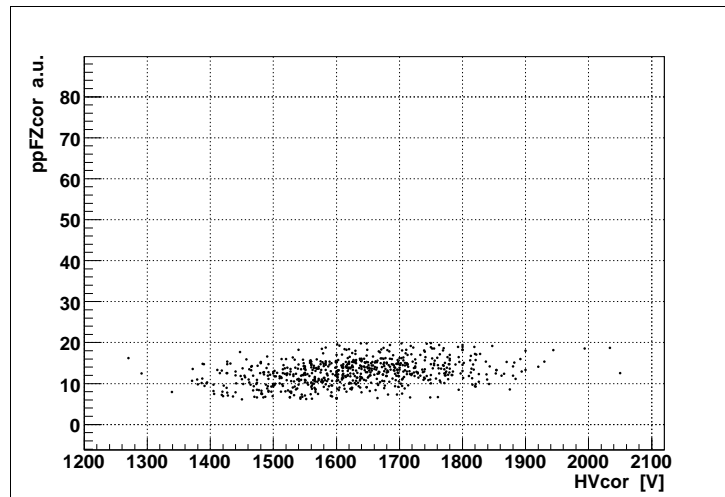


Figure 30: Measured peak position of the crystals versus high voltage after high voltage adjustment.

The peak width $\frac{\sigma}{mean} * 100\%$ for measured crystals was also calculated and is presented in Fig. 31 as a histogram. The histogram is centered around the value of 15%. The peak width is a convolution of the experimental resolution as well the gamma spectrum distribution from used source Fig. 24. The extraction of real crystal resolution is hard to estimate, but the calculated value is quite satisfactory.

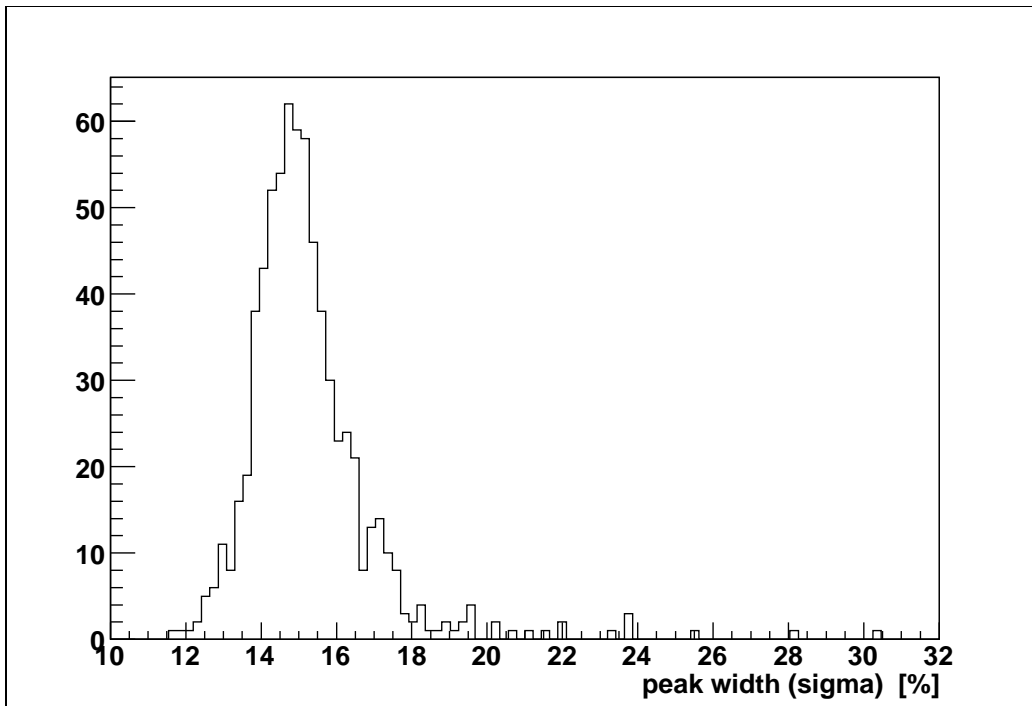


Figure 31: Histogram of measured width (in terms of σ) for different crystals.

4.4 Cosmics measurements

The source tests were supplemented by measuring the response for cosmic muons for a few modules. The electronics setup was the same as described in section 4.1. Five modules at different azimuthal angles (0° , 45° , 90° , 135° , 180°) have been selected Fig. 32. The data were analysed as described in section 4.2.

The GEANT3 based Wasa Monte-Carlo program was used to simulate the shape and the peak position of the energy deposits. Consequently, different geometries and sizes of the crystals were taken into account [21]. The muons were generated accordingly with a zenith angular distribution of $\cos^2(\phi)$ for $\phi = 0^\circ - 80^\circ$.

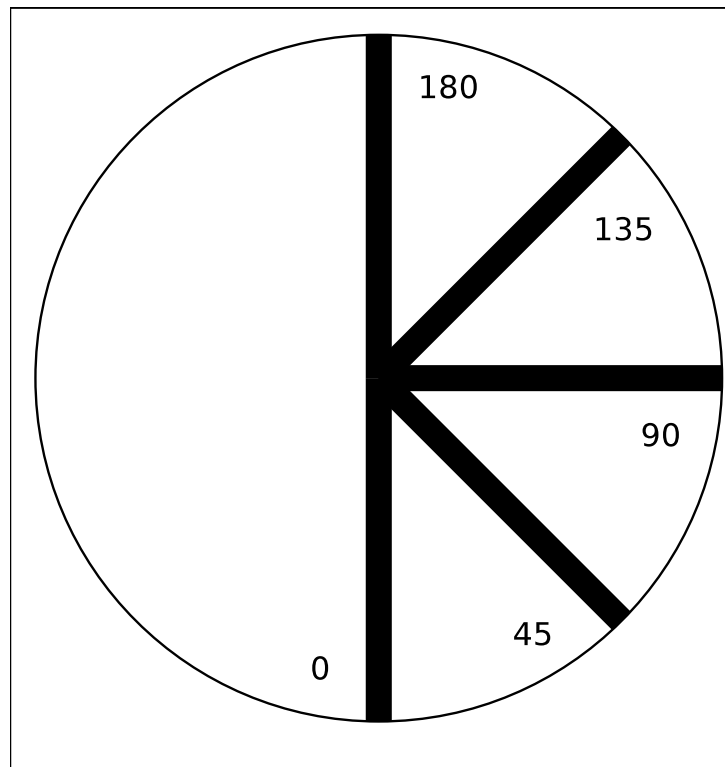


Figure 32: The positions of the tested crystals in the calorimeter.

The simulated spectra for the five different crystals are presented in Fig. 33. The change of the slopes of tails of distributions is expected and can be reproduced by the simulation. This effect is due to the angular orientation of the measured crystal: most of the cosmics are coming from $\phi = 0^\circ$, so for different orientations they penetrate different amount of material. The

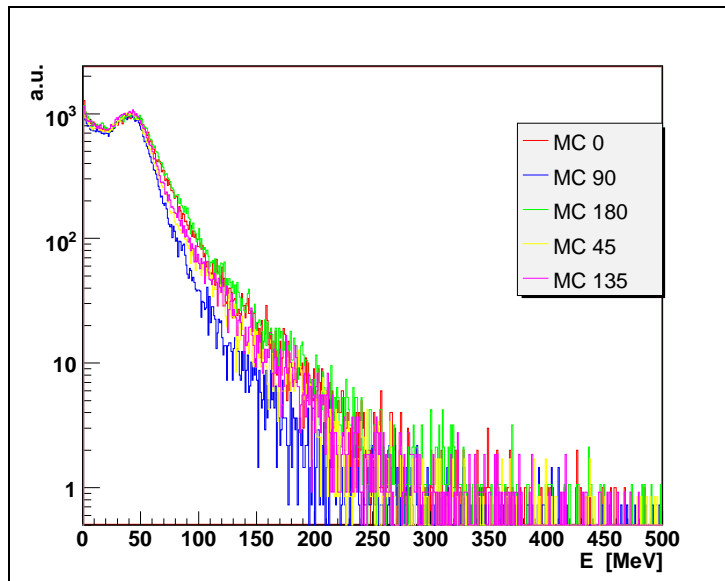


Figure 33: Simulated Monte-Carlo spectra for cosmic muons in five different crystals.

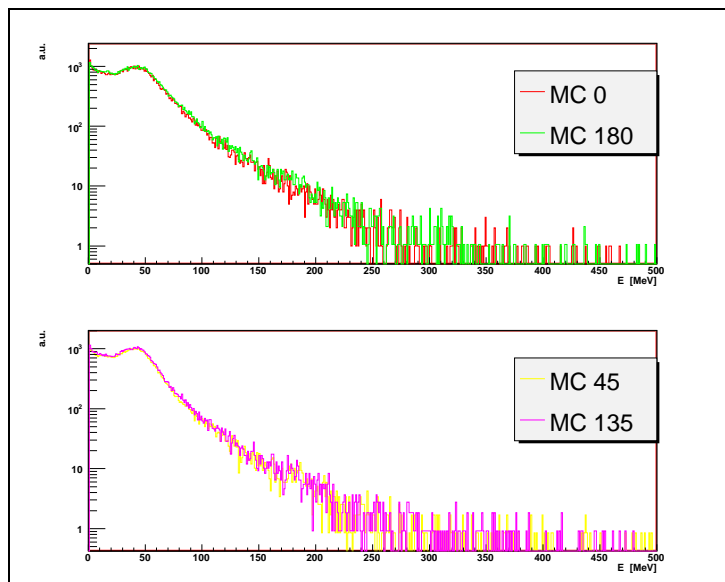


Figure 34: Simulated Monte-Carlo spectra: upper picture shows crystals at angles of 0 and 180, the lower picture at angles of 45 and 135.

symmetry of the distributions should be visible between the crystals oriented opposite the 90° direction. The Fig. 34 shows simulated spectra for crystals oriented opposite to the 90° axis.

The comparison was done to check to what extent the source measurements can be used for calibrating the calorimeter. The measured spectra were calibrated using the peak position from source measurements (section 4.3) and compared to the simulated ones Fig. 35. As one can see, the peak position of the distributions differs: the calibration performed in such a way has a precision of about $\sim 10\%$. The explanation of this effect is as follows: The shower induced by 4.4MeV gammas has its maximum in the crystal at depth of $\sim 3\text{cm}$. The crystals are $\sim 30\text{cm}$ long, so the scintillation light has to pass most of the crystal length, reflecting from the aluminized mylar foil wrapping and attenuating. In case of cosmic muons, the crystal is illuminated from all directions with different intensities, the cosmic are minimum ionizing particles. They penetrate the crystal losing small amount of their energy. This is the reason of differences in peak positions. The precision of arrangement of the source in front of the crystal is also important.

The next step was to check the consistency of the data, to see the expected changes of the slope of the tails. The measured spectra were thus re-calibrated using the peak position from the Monte-Carlo simulation and compared accordingly Fig. 36. In order to see also the symmetry effect between the spectra for crystals oriented opposite the 90° direction, Fig. 37 was plotted. The distributions agree quite well.

To validate also the accuracy of the Monte-Carlo simulation predictions with the performed experiment, the data calibrated using simulation were plotted together with calculated Monte-Carlo spectra for five different crystals respectively Fig. 38, the normalization for peak position was applied for each. One can see the spectra are matching very good each other, the shape is described quite satisfactory, from the peak position up to the tails. The conclusion is that the performed Monte-Carlo simulation for the cosmic muons reproduces well the energy deposits in the CsI(Na) crystals.

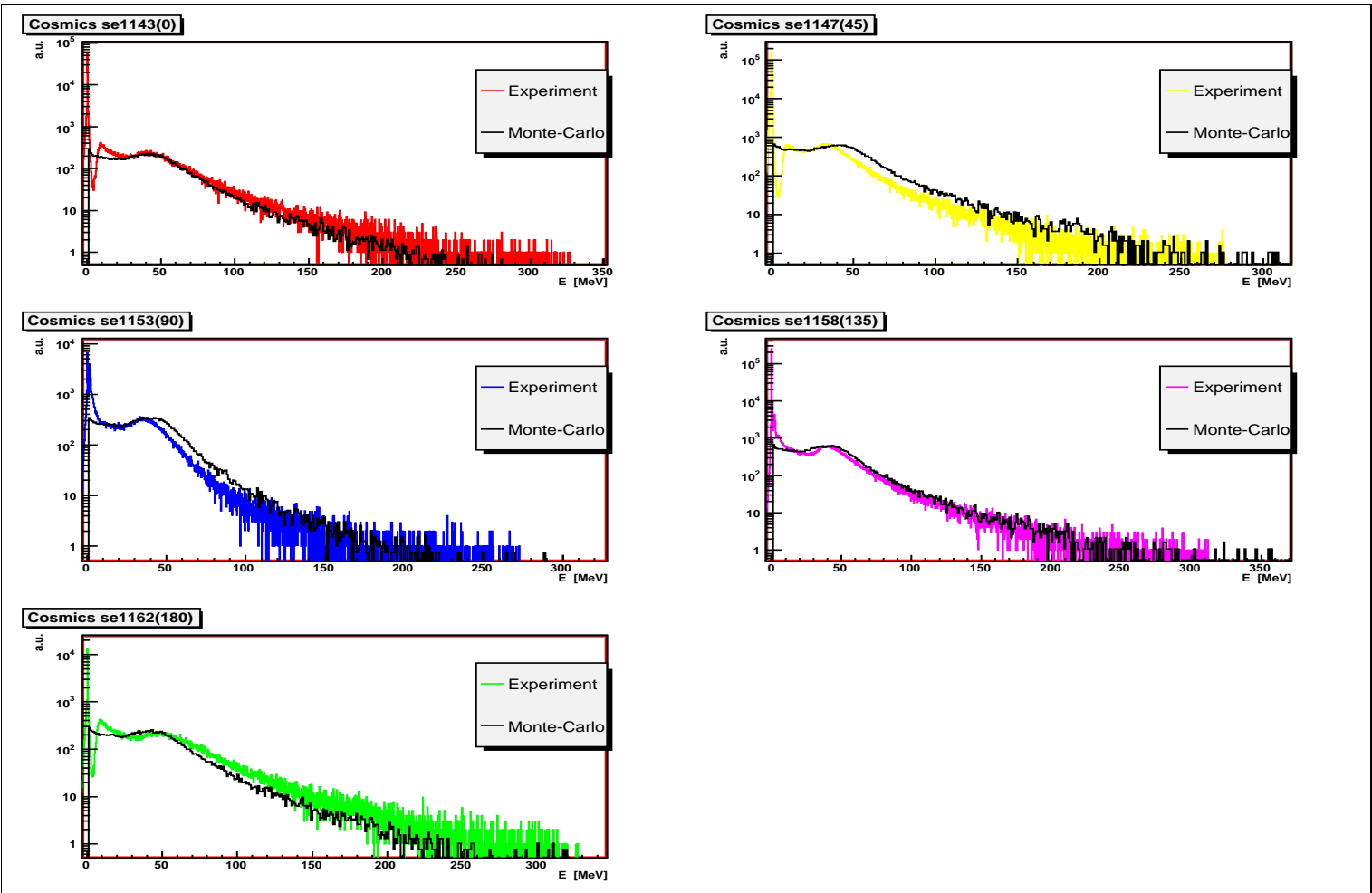


Figure 35: Measured cosmic muons spectra (calibrated by the 4.4MeV gammas) compared to the Monte-Carlo spectra.

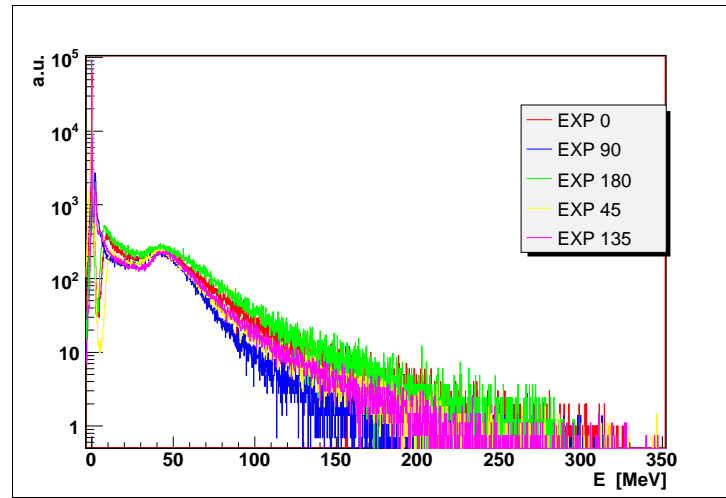


Figure 36: Measured cosmic muons spectra calibrated using the simulated peak position.

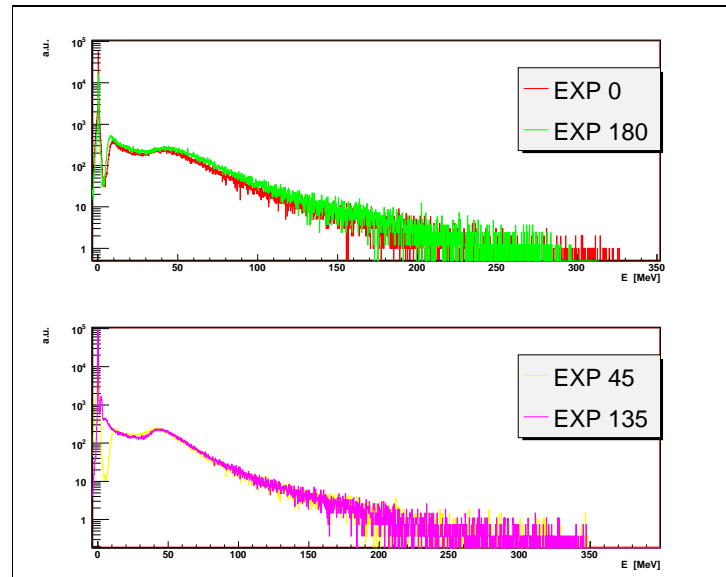


Figure 37: Measured cosmic muons spectra calibrated with simulation: upper picture shows crystals at angles of 0 and 180, the lower picture at angles of 45 and 135.

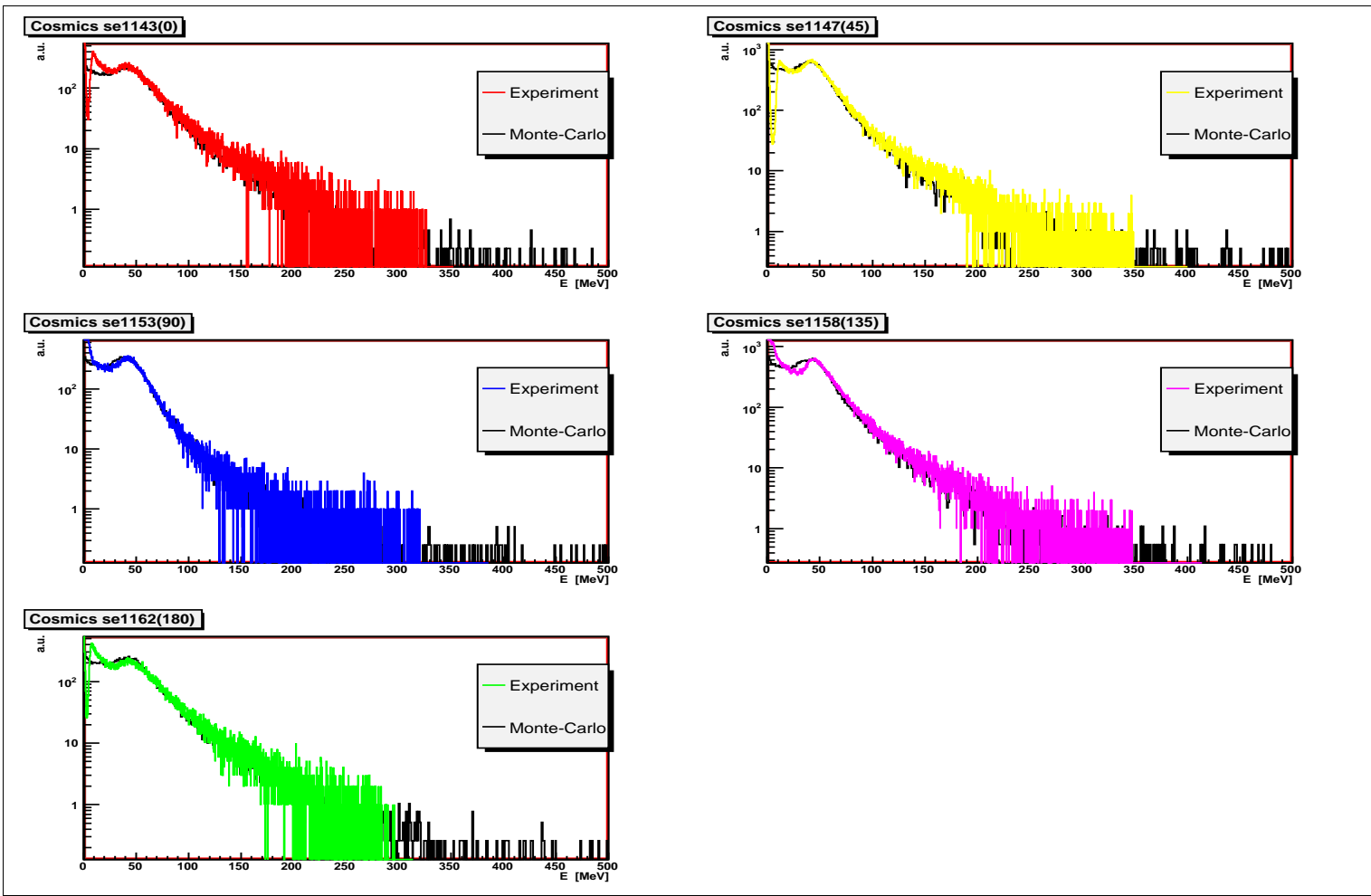


Figure 38: Measured cosmic muons spectra (calibrated by the peak position from simulation) compared to the Monte-Carlo spectra.

5 Summary and conclusions

The tests of the electromagnetic calorimeter components (CsI(Na) crystals) for the WASA at COSY setup were performed. All available modules were tested to check their properties after transport. Scanning of the modules was performed with a radioactive source providing 4.4 MeV gammas. Some broken channels were found, fixed or replaced. The energy calibration constant was calculated for each crystal and the peak width for this energy was extracted (in average 15%). This width is a consequence of the experimental resolution as well the used gamma source spectrum.

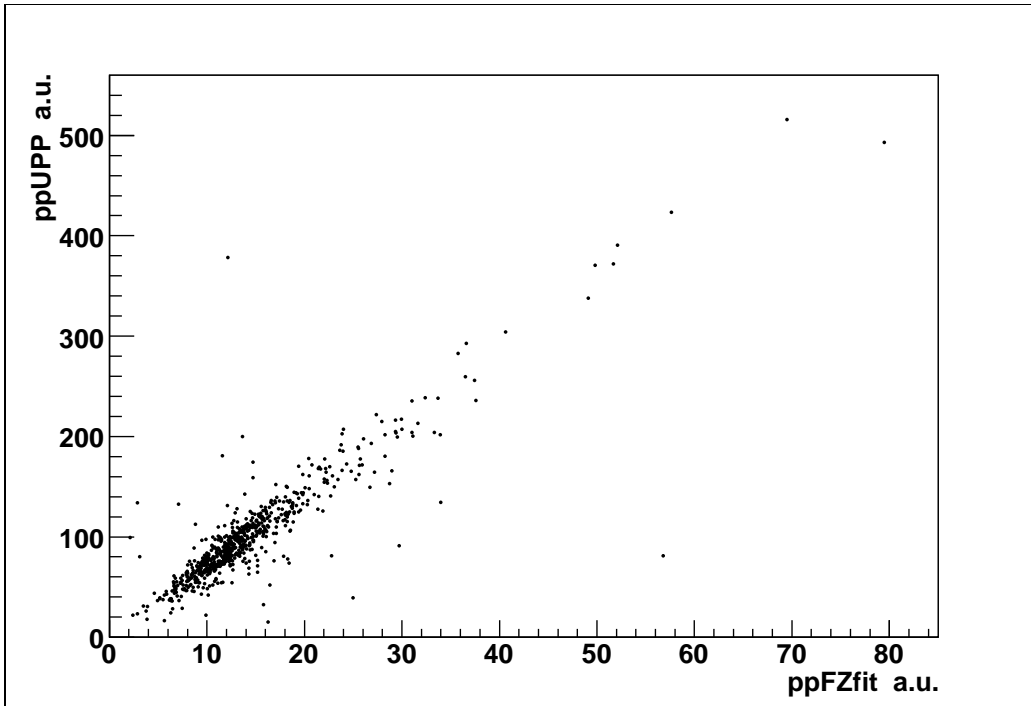


Figure 39: Comparison between peak the positions measured in Uppsala and in Fz-Jülich.

Similar measurements with a source of the same type were done earlier at TSL in Uppsala before moving WASA to IKP at Fz-Jülich [22]. The comparison between the measured peak positions is presented in Fig. 39. In general, strong correlation between these two measurements is observed, but however, in few cases a discrepancy can be seen. The latter may be the result of changed optical contacts between the light guide and the photomultiplier as an effect of the transport. The data are consistent among the measurements,

which proves the same unchanged good quality of the components after the transfer from the CELSIUS ring to the new site.

In addition the task of investigating the energy calibration was done using cosmic muons (see section 4.4). The measured cosmic spectra were compared with the Monte-Carlo simulation. The experimental bias for calibration was determined from this comparison and estimated on the level of $\sim 10\%$. The WASA calorimeter is in satisfactory condition, as it was in the TLS, and it is ready for mounting at the COSY ring and for commissioning in August. Fig. 40 shows the invariant mass of two gammas reconstructed in the electromagnetic calorimeter versus the missing mass of two protons extracted from the forward detector. As seen on the right, peaks of π and η mesons are identified with good energy resolution, which confirms the detection capabilities of WASA. The performed tests of calorimeter prove the feasibility of experiments planned for WASA at COSY starting at the beginning of 2007.

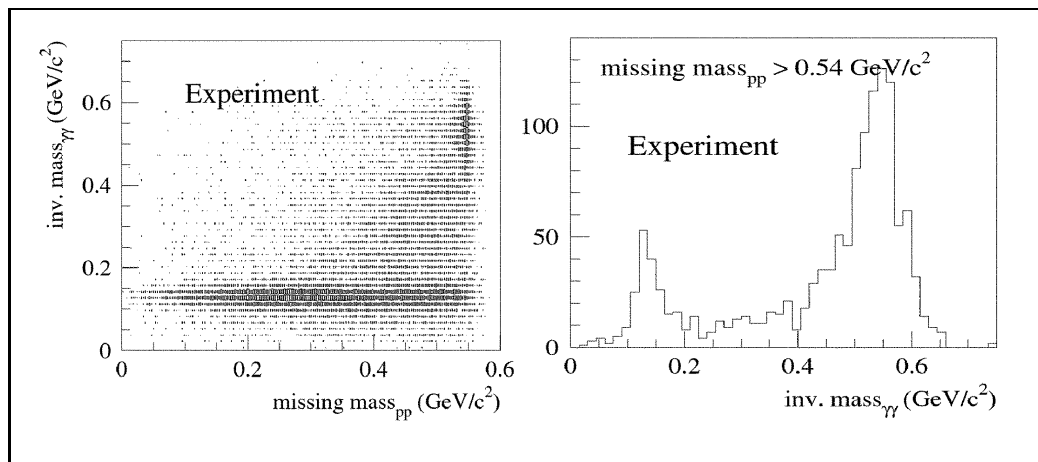


Figure 40: Left picture: Invariant mass of two gammas reconstructed in the calorimeter versus the missing mass of two protons extracted from the forward detector. Right picture: Invariant mass of two gammas with a cut on missing mass; pion and eta peaks are clearly separated [4].

References

- [1] WASA collaboration. *WASA gets a new home at COSY*. CERN courier, January 2005.
- [2] H. H. Adam et al. *Proposal for the Wide Angle Shower Apparatus (WASA) at COSY-Jülich "WASA at COSY"*. Jülich, 2004.
- [3] M. Jacewicz et al. Charged decay products identification possibilities in WASA. *Physica Scripta, Vol. T104*, 2003.
- [4] S. Kullander et al. First results from the CELSIUS/WASA facility. *Nuclear Physics, A721*, 2003.
- [5] J. Zabierowski et al. The CELSIUS/WASA detector facility. *Physica Scripta, T99*, 2002.
- [6] C. Ekström et al. The WASA facility at the CELSIUS storage ring. *TSL-notes, 98-44*, 1998.
- [7] <http://www.fz-juelich.de/ikp/wasa>
- [8] R. Maier. Cooler synchrotron COSY – performance and perspectives. *Nucl. Instr. and Meth. in Phys. Res. A 390*, 1997.
- [9] H. R. Vega-Carrillo E. Manzanares-Acuña A. M. Becerra-Ferreiro A. Carrillo-Nuñez. Neutron and gamma-ray spectra of $^{238}\text{PuBe}$ and $^{241}\text{AmBe}$. *Applied Radiation and Isotopes 57*, 2002.
- [10] P. Moskal. Hadronic Interactions of η and η' mesons with protons. *Jagiellonian University Institute of Physics*, 2004
- [11] D.J. Gross, S.B. Treiman, F. Wilczek. *Phys. Rev. D19 2188*, 1979.
- [12] William R. Leo. *Techniques for Nuclear and Particle Physics Experiments*. Springer-verlang, 1987.
- [13] S. Eidelman et al. Review of particle physics. *Physics letters B 592*, 2004.
- [14] F. Gianotti C. W. Fabjan. Calorimetry for particle physics. *Rev. Mod. Phys., Vol. 75, No. 4*, 2003.
- [15] M. Maire. Proceedings of the 9th International Conference on Calorimetry in HEP (CALOR 2000). *INFN Frascati Physics Series edited by B. Aubert et al.*, Annecy, France, 2001.



-
- [16] R. Novotny R. Beck W. Döring V. Hejny M. Hoek A. Hofstaetter V. Metag K. Römer. Scintillators for photon detection at medium energies – a comparative study of BaF₂, CeF₃ and PbWO₄. *Nucl. Instr. and Meth. in Phys. Res. A* 486, 2002.
- [17] R. Wigmans C. W. Fabjan. Energy measurement of elementary particles. *Rev. Prog. Phys.*, Vol. 52, 1989.
- [18] Donald H. Perkins. *Introduction to high energy physics*. Press Syndicate of the Cambridge, 2000.
- [19] <http://root.cern.ch>
- [20] V. Hejny M. Hartmann A. Mussgiller. *RootSorter: A new analysis framework for ANKE*. IKP Fz-Jülich Annual report, 2002.
- [21] I. Koch Measurement of $2\pi^0$ and $3\pi^0$ Production in Proton-Proton Collisions at a Center of Mass Energy of 2.465GeV. *Uppsala Universitet*, 2004
- [22] David Duniec. *Measurements of SEC with source in TSL Uppsala*. Private communication, david.duniec@ts1.uu.se



Appendix A

Table a: Results from test with $^{241}\text{AmBe}$ source

cable	peak position [a.u.]	peak sigma [a.u.]	high voltage [V]
459	14.18	1.98	1615
460	12.37	1.59	1521
461	13.29	2.18	1900
462	15.45	2.24	1575
463	7.87	1.13	1440
464	10.31	1.49	1550
465	11.51	1.7	1640
466	12.4	1.94	1639
467	11.3	1.67	1510
470	6.67	1.06	1526
471	12.38	1.73	1720
472	14.8	2.19	1620
473	19.81	2.73	1639
474	18.42	2.48	1613
475	16.22	2.51	1703
476	13.68	1.97	1622
477	15.1	2.1	1620
478	11.15	1.7	1572
479	17.11	2.61	1719
483	15.09	1.97	1480
484	15.42	2.05	1583
485	13.23	1.78	1465
486	13.89	2.04	1535
487	11.03	1.55	1587
488	11.63	1.66	1566
489	13.75	1.99	1650
490	14.94	2.05	1480
491	13.12	1.8	1610
492	14.14	2.05	1640
493	18.84	3.4	1750
494	10.92	1.68	1644
495	14.73	2.02	1750
496	14.9	2.4	1680
497	14.83	2.24	1695

Continued on next page



Table a – continued from previous page

cable	peak position [a.u.]	peak sigma [a.u.]	high voltage [V]
498	15.77	2.19	1638
499	14.24	1.83	1466
500	16.19	2.52	1678
501	14.98	2.19	1592
502	7.99	1.3	1616
503	12.66	1.82	1633
504	13.42	2.44	1587
507	13.71	2.02	1518
508	10.95	1.43	1538
510	12.9	1.91	1785
511	15.31	2.09	1599
512	12.55	1.74	1415
513	12.68	1.88	1575
514	13.74	2	1451
515	7.61	1.12	1481
516	14.19	2.08	1640
517	7.82	1.09	1427
518	14.5	2.07	1560
519	19.42	2.41	1763
520	13.16	1.85	1631
521	15.6	2.26	1665
522	16.39	2.29	1531
523	14.07	1.89	1465
524	14.63	2.04	1560
525	14.63	2.05	1540
526	14.95	2.1	1670
527	15.3	2.19	1480
528	12.78	1.84	1692
531	12.41	1.74	1665
532	18.49	2.6	1577
533	13.98	2.02	1560
534	6.96	1.06	1499
535	12.76	1.8	1485
536	11.87	1.69	1614
537	11.45	1.74	1739
538	15.69	2.21	1559
539	11.58	1.66	1512
540	13.12	1.88	1618
Continued on next page			

Table a – continued from previous page

cable	peak position [a.u.]	peak sigma [a.u.]	high voltage [V]
541	13.46	1.78	1462
542	9.07	1.34	1531
543	12.86	1.87	1500
544	8.35	1.29	1468
545	18.53	3.05	1755
546	15.99	2.3	1688
547	14.06	1.95	1624
548	11.25	1.57	1387
549	17.17	2.41	1764
550	10.2	1.44	1474
551	10.77	1.65	1626
555	18.42	2.16	1620
556	7.11	1.04	1550
557	15.28	2.04	1625
558	11.15	1.57	1492
559	9.05	1.41	1638
560	18	2.47	1630
561	12.49	1.84	1500
562	12.09	1.68	1546
563	13.9	2.01	1598
564	10	1.43	1620
565	12.27	1.68	1485
567	15.78	2.16	1603
568	15.99	2.36	1520
569	15.14	2.24	1661
570	16.21	2.12	1618
571	11.4	1.63	1566
572	14.64	2.13	1690
573	14.18	2.07	1625
574	18.92	2.89	1793
575	14.7	2.08	1390
579	15.36	2.35	1930
580	14.46	2.21	1705
581	7.49	1.11	1482
582	11.93	1.69	1880
584	12.36	1.79	1518
585	10.29	1.43	1395
586	8.38	1.25	1604

Continued on next page



Table a – continued from previous page

cable	peak position [a.u.]	peak sigma [a.u.]	high voltage [V]
587	14.39	2.04	1638
588	10.82	1.74	1582
589	18.82	3.3	1722
590	15.19	2.21	1599
591	11.17	1.7	1884
592	16.1	2.28	1670
593	19.71	2.94	1743
594	11.94	1.83	1733
595	15.66	2.25	1706
596	10.17	1.59	1621
597	16.74	2.62	1813
598	12.91	1.97	1894
600	13.03	1.97	1672
603	10.83	1.84	1521
604	13.86	2.1	1725
605	10.69	1.55	1593
606	10.03	1.41	1510
607	8.38	1.35	1477
608	11.95	1.82	1491
609	11.85	1.98	1743
610	13.29	1.92	1583
611	14.45	2.11	1691
612	11.05	1.69	1566
613	14.72	2.06	1688
614	8.08	1.3	1519
615	6.65	0.99	1717
616	19.85	3.16	1600
617	12.56	1.93	1698
618	12.71	1.95	1680
619	9.32	1.6	1693
620	12.9	2.03	1739
621	15.66	2.24	1812
622	9.25	1.58	1821
624	14.07	2.3	1762
627	6.34	0.96	1561
628	15	2.21	1655
629	15.9	2.14	1725
630	12.83	1.65	1682
Continued on next page			

Table a – continued from previous page

cable	peak position [a.u.]	peak sigma [a.u.]	high voltage [V]
631	13.49	1.89	1544
632	17.8	2.5	1740
633	8.28	1.17	1481
634	14.76	2.3	1700
635	13.79	1.99	1636
636	11.64	1.72	1615
637	10.12	1.65	1771
638	15.45	2.28	1640
639	10.29	1.65	1578
640	12.71	1.84	1697
641	15.58	2.52	1756
642	13.32	2.12	1697
643	12.2	1.93	1603
644	8.86	1.5	1676
645	13.01	2.1	1600
646	14.18	2.41	1843
647	15.11	2.64	1882
649	12.71	2.18	1745
650	6.59	0.98	1484
651	12.28	1.67	1826
652	17.22	2.36	1828
653	10.25	1.55	1560
654	10.24	1.76	1655
655	14.77	2.15	1697
656	9.41	1.55	1515
657	14.38	2.09	1656
658	12.56	1.94	1479
659	12.92	1.87	1774
660	16.12	2.41	1672
661	13.59	2.07	1550
662	13.85	2.16	1582
663	14.38	2.14	1582
665	12.84	1.92	1727
666	14.96	2.41	1631
667	16.96	2.53	1600
668	13.94	2.2	1645
669	14.85	2.34	1755
670	19.15	2.94	1847

Continued on next page



Table a – continued from previous page

cable	peak position [a.u.]	peak sigma [a.u.]	high voltage [V]
671	14.84	2.28	1580
796	13.66	1.83	1570
797	10.59	1.58	1600
798	16.25	2.48	1270
800	14.84	2.17	1388
801	11.18	1.64	1758
802	12.81	1.88	1737
803	14.71	2.11	1713
804	12.56	1.78	1561
805	14.52	2.26	1761
808	11.07	1.65	1638
810	11.03	1.57	1777
811	14.67	2.17	1817
812	11.47	1.69	1602
813	8.95	1.43	1624
814	18.73	2.6	1675
815	10.68	1.64	1631
816	15.07	2.1	1558
817	9.9	1.47	1500
819	11.32	1.66	1815
820	9.37	1.37	1469
821	8.5	1.29	1474
822	15.03	2.09	1772
823	15.18	2.56	1664
824	15.52	2	1599
825	13.57	2.13	1372
826	9.63	1.44	1502
827	14.28	2.14	1548
828	17.63	2.72	1669
830	15.28	2.43	1648
831	13.6	1.96	1539
832	14.7	2.17	1427
833	12.1	1.92	1618
834	6.89	1.33	1420
837	10.83	1.79	1746
838	15.3	2.16	1795
839	6.25	1.02	1552
840	12.18	1.94	1610
Continued on next page			

Table a – continued from previous page

cable	peak position [a.u.]	peak sigma [a.u.]	high voltage [V]
841	14.09	2	1600
842	17.35	2.41	1579
843	15.81	2.04	1547
844	12.69	2.1	1758
846	11.99	1.67	1654
847	19.43	2.79	1685
848	15.39	2.04	1427
849	6.46	1.02	1665
850	14.25	1.95	1549
851	11.12	1.47	1540
852	13.41	1.95	1686
853	13.06	1.73	1567
854	6.85	1.05	1436
855	12.39	1.75	1536
856	14.54	2.1	1583
857	18.24	2.31	1540
858	14.42	1.97	1709
859	15.34	2.2	1626
860	14.73	2.1	1611
861	14.35	1.94	1770
862	15.67	2.12	1740
863	15.76	2.13	1640
864	14.97	2.1	1702
865	14.31	1.93	1475
866	12.07	1.68	1548
867	15.19	2.03	1628
868	14.36	2.07	1622
869	9.97	1.53	1503
870	14.12	2.15	1572
871	7.49	1.17	1571
872	13.9	1.9	1522
873	12.13	1.75	1599
874	13.15	2.02	1652
875	10.8	1.56	1572
876	11.82	1.73	1557
877	16.13	2.25	1752
878	8.99	1.36	1426
879	17.84	2.59	1667

Continued on next page



Table a – continued from previous page

cable	peak position [a.u.]	peak sigma [a.u.]	high voltage [V]
880	8.01	1.19	1526
881	10.63	1.54	1528
882	13.06	1.94	1502
883	12.23	1.8	1532
884	12.31	1.7	1554
885	12.74	1.93	1492
886	13.95	1.95	1618
888	15.26	2.03	1657
889	11.91	1.76	1454
890	15.74	2.14	1627
891	7.46	1.1	1406
893	12.3	1.7	1717
894	14.34	2.19	1610
895	13.62	1.9	1619
896	14.19	2.08	1644
897	13.97	2.12	1692
898	10.42	1.54	1570
899	11.78	1.71	1622
900	14.41	2	1608
901	12.36	1.67	1585
902	14.48	2.13	1516
903	14.45	1.95	1658
904	10.05	1.44	1394
905	13.25	1.97	1645
906	9.94	1.45	1562
907	12.23	1.86	1674
908	9.75	1.51	1464
909	16.61	2.38	1490
910	14.48	2.17	1755
911	15.11	2.29	1680
912	12.43	1.71	1549
913	7.71	1.19	1528
914	16.04	2.39	1637
915	15.22	2.16	1650
917	11.18	1.89	1740
918	7.33	1.1	1682
919	12.88	1.89	1600
920	15.32	2.38	1560

Continued on next page

Table a – continued from previous page

cable	peak position [a.u.]	peak sigma [a.u.]	high voltage [V]
921	11.87	1.81	1610
922	11.17	1.65	1664
924	8.96	1.36	1625
925	12.69	1.92	1813
926	7.26	1.15	1418
927	14.94	2.37	1712
928	18.3	2.73	1800
929	10.32	1.55	1669
930	11	1.87	1749
931	12.06	1.89	1750
932	15.62	2.31	1627
933	18.55	2.93	1752
934	13.6	2	1814
935	13.63	2.04	1766
936	9.87	1.54	1821
937	15.53	2.32	1558
938	15.1	2.3	1676
940	14.45	2.28	1729
941	12.45	1.99	1763
943	17.26	3.16	1820
944	14.64	2.27	1713
945	18.26	2.54	1711
946	8.59	1.31	1586
947	15.04	2.01	1646
948	10.43	1.55	1684
949	13.3	1.97	1411
950	13.46	1.97	1740
951	11.48	1.77	1632
952	11.48	1.75	1730
953	10.02	1.55	1623
954	6.67	1.21	1761
955	8.47	1.45	1794
956	14.29	2.2	1676
957	12.92	2.04	1712
958	10.35	1.72	1765
959	17	2.57	1780
960	11.18	3.39	1705
961	13.3	1.92	1626

Continued on next page



Table a – continued from previous page

cable	peak position [a.u.]	peak sigma [a.u.]	high voltage [V]
962	12.25	1.85	1838
964	13.16	2.05	1782
965	13.66	2.03	1656
966	12.16	2.11	1777
967	16.02	2.2	1780
968	15.03	2.22	1709
969	15.3	2.45	1615
970	12	1.84	1653
971	13.58	1.8	1678
972	14.49	2.24	1769
973	7	1.16	1591
974	13.21	2.14	1691
975	13.86	2.91	1664
976	15.74	2.4	1821
977	8.93	1.38	1565
978	8.44	1.27	1662
979	11.77	1.88	1656
980	10.04	1.63	1750
981	17.73	3.02	1447
982	18.74	2.82	2034
983	18.52	2.88	1994
984	9.1	1.55	1648
985	11.83	1.73	1698
986	13.66	2	1653
987	15.18	2.2	1600
988	12.87	2.07	1698
990	18.94	3.13	1819
991	14.63	2.07	1700
992	15.8	2.3	1534
993	13.85	2	1621
994	13.77	1.97	1568
995	13.88	1.95	1616
996	11.05	1.62	1450
997	19.18	2.95	1718
998	8.34	1.36	1523
999	8.23	1.32	1492
1000	11.92	1.91	1618
1001	7.44	1.45	1481
Continued on next page			

Table a – continued from previous page

cable	peak position [a.u.]	peak sigma [a.u.]	high voltage [V]
1002	13.8	2.84	1935
1003	13.45	2.12	1985
1005	15.9	2.56	1569
1006	15.96	2.58	1892
1007	13.69	2.2	1753
1008	14.14	2.74	1920
1009	14.16	2.94	1880
1010	8.05	1.44	1497
1011	6.31	1.27	1543
1013	11.95	1.95	1695
1014	15.06	2.56	1802
1015	13.1	1.8	1800
1016	8.05	1.52	1528
1017	16.08	2.33	1685
1018	14.74	2.16	1779
1019	11.67	1.75	1638
1020	13.87	2.41	1700
1021	14.69	2.15	1675
1022	16.61	2.33	1658
1023	11.99	1.75	1772
1024	13.36	2.03	1576
1025	8	1.27	1492
1026	13.91	2.37	1925
1027	11.41	1.84	1668
1028	13.51	2.34	1771
1142	12.62	2.77	1550
1143	12.5	1.88	1771
1144	12.68	1.99	1484
1145	10.46	1.56	1576
1146	13.22	1.95	1709
1147	13.87	2.11	1693
1148	10.6	1.56	1541
1149	15.86	2.62	1457
1150	11.82	2.09	1724
1151	8.71	1.49	1622
1152	16.44	2.55	1794
1153	13.42	1.94	1736
1154	13.05	2.26	1603

Continued on next page



Table a – continued from previous page

cable	peak position [a.u.]	peak sigma [a.u.]	high voltage [V]
1155	12.85	2.04	1792
1156	9.33	1.58	1635
1157	13.05	2.15	1716
1158	11.84	1.78	1629
1159	15.71	2.43	1697
1160	10.46	1.81	1826
1161	13.14	2.24	1692
1162	12.7	2	1723
1164	12.86	2.07	1748
1166	12.25	1.97	1526
1167	9.32	1.48	1588
1168	13.92	2	1610
1169	10.75	1.73	1647
1170	12.42	1.71	1611
1172	11.51	1.67	1455
1175	13.15	1.97	1656
1176	12.39	1.96	1693
1178	10.87	1.66	1544
1179	16.33	2.47	1706
1180	11.01	1.77	1609
1181	12.43	2.07	1729
1182	15.29	2.21	1698
1183	13.88	2.01	1652
1184	10	1.65	1702
1186	10.87	1.73	1474
1187	18.06	2.64	1704
1188	8.54	1.32	1875
1190	13.78	2	1762
1192	14.01	2.11	1626
1193	14.55	1.98	1617
1194	9.48	1.42	1561
1195	11.02	2.01	1577
1196	11.3	1.6	1641
1197	9.52	1.46	1677
1198	11.81	1.84	1679
1199	9.62	1.7	1666
1200	12.06	1.81	1719
1201	14.66	2.11	1712

Continued on next page

Table a – continued from previous page

cable	peak position [a.u.]	peak sigma [a.u.]	high voltage [V]
1202	10.72	1.52	1577
1203	11.35	1.82	1801
1204	18.05	2.7	1769
1205	6.61	1.28	1749
1206	11.86	1.93	1680
1207	10.93	1.66	1550
1208	14.18	2.07	1725
1209	14.81	2.08	1560
1210	9.21	1.43	1560
1211	16.53	2.37	1621
1212	10.56	1.73	1585
1213	14.33	2.17	1569
1214	15.19	2.28	1714
1216	18.16	2.76	1681
1217	8.21	1.25	1653
1218	9.09	1.5	1648
1219	6.75	1.1	1470
1220	12.33	1.72	1712
1221	18.14	2.88	1800
1222	14.67	2.16	1789
1223	13.43	2.02	1700
1224	13.79	2.02	1550
1225	6.79	1.01	1487
1226	13.32	2.02	1551
1227	9.76	1.45	1488
1228	15.48	2.2	1630
1229	11.24	1.8	1689
1230	6.59	1.08	1474
1231	15.35	2.21	1620
1232	11.44	1.85	1650
1233	12.43	1.94	1622
1234	14.15	2.32	1587
1235	14.46	2.16	1651
1236	16	2.39	1513
1237	9.29	1.5	1534
1238	13.19	2.11	1686
1240	15.81	2.04	1639
1241	14.24	1.95	1580

Continued on next page



Table a – continued from previous page

cable	peak position [a.u.]	peak sigma [a.u.]	high voltage [V]
1242	9.61	1.37	1592
1243	10.51	1.44	1699
1244	12.61	1.8	1506
1245	10.79	1.6	1603
1246	11.34	1.6	1580
1247	9.19	1.35	1580
1248	10.27	1.52	1462
1249	12.8	2.18	1668
1250	9.23	1.34	1500
1251	6.44	0.99	1600
1252	12.15	1.67	1600
1253	13.54	2.16	1640
1254	10.91	1.79	1738
1255	11.28	1.61	1609
1256	10.66	1.63	1673
1257	12.58	1.71	1515
1258	16.28	2.31	1760
1259	9.61	1.45	1500
1260	7.88	1.3	1592
1261	8.58	1.21	1624
1262	14.48	2.33	1914
1264	7.16	1.15	1533
1265	11.84	1.78	1448
1266	8.75	1.36	1561
1267	11.85	1.74	1532
1268	12.8	1.8	1647
1269	10.03	1.36	1441
1270	13.66	2.17	1780
1271	12.95	1.81	1440
1272	13.8	2.04	1564
1273	18.82	2.63	1583
1274	14.03	2.38	1609
1276	13.6	1.85	1572
1277	10.18	1.58	1634
1278	8.02	1.12	1419
1279	17.05	2.43	1609
1280	13.84	2.05	1775
1281	14.92	2.1	1432

Continued on next page

Table a – continued from previous page

cable	peak position [a.u.]	peak sigma [a.u.]	high voltage [V]
1282	9.46	1.42	1391
1283	14.54	2.38	1800
1284	14.38	2.07	1625
1285	16.97	2.44	1733
1286	13.33	2.05	1660
1288	12.71	1.86	1729
1289	11.88	1.77	1600
1290	19.58	2.95	1601
1291	6.75	1.12	1546
1292	9.46	1.53	1704
1293	13.05	1.92	1676
1294	9.49	1.46	1421
1295	12.45	1.8	1522
1296	10.23	1.62	1554
1297	11.74	1.63	1510
1298	8.8	1.35	1538
1299	12.3	1.81	1594
1300	12.56	1.87	1427
1301	12.03	1.71	1598
1302	11.76	1.68	1504
1303	13.55	1.9	1527
1304	11.4	1.58	1513
1305	9.49	1.41	1593
1306	19.25	3.01	1605
1307	12.5	1.75	1291
1308	13.67	1.94	1549
1309	14.55	2.17	1680
1310	15.24	2.2	1542
1312	6.81	1.13	1593
1313	9.76	1.43	1500
1314	16.05	2.36	1640
1315	12.68	2.21	1779
1316	11.1	1.74	1540
1318	17.21	2.73	1630
1319	12.55	2.92	2050
1320	7.57	1.37	1704
1321	16.89	2.73	1690
1322	11.76	2.04	1502

Continued on next page



Table a – continued from previous page

cable	peak position [a.u.]	peak sigma [a.u.]	high voltage [V]
1323	18.23	2.58	1649
1324	15.77	2.13	1631
1325	11.9	2.09	1468
1326	16.02	2.3	1675
1327	8.68	1.51	1567
1328	10.67	1.56	1565
1329	15.35	2.35	1589
1330	7.39	1.24	1559
1331	14.73	2.25	1575
1332	6.43	1.29	1600
1333	13.79	2.07	1682
1415	12.64	1.95	1600
1416	12.04	1.87	1783
1417	13.86	2.05	1610
1418	13.35	1.99	1854
1419	9.15	1.47	1698
1420	12.38	2	1866
1421	12.44	1.77	1667
1422	15.74	2.82	1855
1423	9.93	1.44	1564
1424	13.4	2.21	1818
1425	14.02	2.19	1649
1426	18.07	2.59	1739
1427	6.6	1.03	1543
1428	17.36	2.47	1710
1429	11.41	1.71	1581
1430	9.72	1.48	1555
1431	15.63	2.47	1780
1432	11.84	2.17	1810
1433	12	1.88	1773
1434	9.94	1.63	1665
1435	14.36	2.25	1564
1436	9.38	1.45	1820
1437	13.85	2.08	1611
1438	15.18	2.21	1645
1439	9.8	1.68	1631
1440	15.26	2.35	1870
1441	18.66	2.91	1770

Continued on next page

Table a – continued from previous page

cable	peak position [a.u.]	peak sigma [a.u.]	high voltage [V]
1442	8.48	1.25	1567
1443	10.36	1.7	1606
1444	10.97	1.9	1704
1446	13.21	2.3	1855
1447	12.65	1.91	1745
1449	12.68	1.97	1654
1450	14.49	2.09	1683
1451	11.95	1.71	1544
1452	14.03	2.21	1672
1453	12.05	1.81	1784
1454	16.23	2.36	1700
1455	15.35	3.3	1837
1456	8.82	1.42	1708
1457	14.7	2.19	1778
1458	13.19	2.02	1418
1459	11.46	1.79	1633
1460	10.75	1.71	1764
1461	12.49	1.9	1797
1462	6.27	1.19	1600
1463	12.36	2.01	1585
1464	11.9	2.08	1862
1465	19.86	3.14	1750
1466	12.46	2.17	1853
1468	18.92	2.7	1800
1470	14.45	2.46	1712
1471	8.81	1.35	1490
1472	14.66	2.17	1589
1473	15.28	2.19	1630
1474	10.97	2.14	1839
1475	18.32	2.57	1671
1476	13.54	2.03	1660
1478	9.89	1.75	1842
1479	13.23	1.91	1854
1480	8.72	1.36	1613
1481	18.25	2.64	1616
1482	9.54	1.55	1714
1483	7.32	1.25	1696
1484	13.14	2.04	1681

Continued on next page



Table a – continued from previous page

cable	peak position [a.u.]	peak sigma [a.u.]	high voltage [V]
1485	15.37	2.51	1721
1486	15.27	2.25	1600
1487	11.59	2.26	1707
1488	10.56	1.46	1676
1489	19.83	2.97	1703
1490	12.36	2.1	1627
1491	17.86	2.6	1684
1492	7.07	1.18	1428
1493	10.12	1.54	1629
1494	15.97	2.23	1582
1495	12.08	1.73	1618
1496	10.81	1.8	1694
1497	7.87	1.22	1640
1498	15.06	2.28	1583
1499	13.05	1.83	1591
1500	13.44	2.02	1663
1501	7.98	1.12	1512
1502	14.13	2.01	1714
1503	14.07	1.99	1685
1504	9.03	1.44	1605
1505	12.62	1.64	1773
1506	14.18	2.14	1550
1507	13.41	1.9	1696
1508	12.16	1.66	1660
1509	13.77	2.03	1723
1510	14.93	2.13	1548
1511	13.3	1.94	1562
1512	19.39	2.86	1800
1513	15.63	2.32	1640
1514	9.27	1.22	1497
1515	10.84	1.59	1563
1516	17.02	2.35	1713
1517	12.42	1.95	1568
1518	14.96	2.26	1712
1519	10.51	1.43	1533
1520	9.59	1.55	1612
1521	8.59	1.29	1536
1522	11.41	1.73	1611
Continued on next page			

Table a – continued from previous page

cable	peak position [a.u.]	peak sigma [a.u.]	high voltage [V]
1523	7.92	1.23	1567
1524	15.16	2.23	1578
1525	15.41	2.24	1662
1526	9.75	1.5	1405
1527	10.55	1.86	1567
1528	13.82	2.13	1489
1529	9.78	1.46	1380
1530	16.09	2.15	1644
1531	10.76	1.64	1637
1532	10.78	1.52	1551
1532	12.17	1.7	1551
1534	12.19	1.78	1495
1535	11	1.72	1461
1536	10.96	1.53	1379
1537	17.46	2.33	1625
1538	7.93	1.27	1339
1539	12.19	1.92	1674
1540	16.83	2.44	1648
1541	6.15	0.93	1450
1542	14.43	2.16	1658
1543	12.05	1.77	1521
1544	10.69	1.57	1371
1545	10.49	1.55	1579
1546	14.99	2.23	1726
1547	13.63	2.05	1569
1548	13.51	1.94	1515
1549	16.46	2.24	1776
1550	8.2	1.25	1405
1551	12.97	1.89	1527
1552	9.38	1.29	1491
1553	13.18	2.01	1602
1554	9.85	1.51	1514
1555	9.79	1.53	1583
1557	9.92	1.58	1452
1558	12	1.72	1586
1559	14.7	2.16	1492
1560	14.61	2.1	1620
1561	6.63	1.02	1526

Continued on next page



Table a – continued from previous page

cable	peak position [a.u.]	peak sigma [a.u.]	high voltage [V]
1562	11.64	1.67	1602
1563	8.69	1.29	1601
1564	14.56	2.21	1701
1565	15.41	2.2	1700
1566	16.04	2.33	1588
1568	11.7	1.81	1651
1569	7.31	1.14	1545
1570	18	3.32	1900
1571	18.16	2.65	1944
1572	13.22	2.03	1604
1573	19.78	3.36	1648
1574	9.72	1.59	1816
1575	13.15	1.98	1603
1576	14.79	2.17	1696
1577	12.01	1.9	1440
1578	10.1	1.74	1386
1579	16.43	2.51	1741
1580	12.51	1.89	1426
1581	12.88	2	1667
1582	11.77	1.83	1699
1583	9.77	1.61	1540
1584	14	2.11	1661
1585	12.94	1.96	1706
1586	9.87	1.69	1473
1587	13.7	2.09	1762
1588	17.1	2.61	1822
1589	14.69	2.47	1742

Acknowledgements

Here I would like to thank all people that helped me to create this thesis and without whom it wouldn't have been possible. I am not able to express my gratitude with my English, I will try my best.

First of all I would like to thank my supervisor Dr. hab. Zbigniew Rudy for introducing me the secrets of data analysis and for time spent on discussions, his guidance was always present.

I am also gratefully to Dr. Volker Hejny, my tutor during the stay in Jülich, for showing me interesting aspects of calorimeter physics and for our fruitfull discussions and, of course, for new definition of common words. I would like to thank Volker as well for being the indispensable source of information concerning experimental physics. Thank You for patience!

I would like also to thank Prof. Hans Ströher for possibility of stay in Forschungszentrum-Jülich and for giving me the opportunity to work with WASA at COSY collaboration.

I am also very grateful to Prof. Reinhard Kulessa for allowing me to prepare this thesis in the Nuclear Physics Department of the Jagiellonian University.

I want to express my appreciation to Prof. Lucjan Jarczyk, Prof. Bogusław Kamys and Prof. Ewa Gudowska-Nowak for their support of my stay in Forschungszentrum.

I also thank all colleagues from WASA at COSY collaboration. It was a pleasure for me to work with You.

I thank my colleagues in IKP: Alexey Dzyuba, Dieter Oellers for the joy of daily work.

I thank also Pawel Podkopal and Michał Janusz for a great time outside the institute.

I also want to express my gratitude to my mother Aniela and father Gerard and brother Michał(Leniwiec) and the rest of my Family, especially granny Rozalia and aunt Bożena for their great love, delicious meals and support through five years of studies in Cracow. Thank You!

